

RESEARCH ARTICLE | AUGUST 02 2023

## Budgets of Reynolds stresses in film cooling with fan-shaped and cylindrical holes

Muting Hao (郝苜婷)  ; Luca di Mare 



*Physics of Fluids* 35, 086103 (2023)

<https://doi.org/10.1063/5.0140670>



CrossMark

# Budgets of Reynolds stresses in film cooling with fan-shaped and cylindrical holes

Cite as: Phys. Fluids **35**, 086103 (2023); doi: [10.1063/5.0140670](https://doi.org/10.1063/5.0140670)

Submitted: 29 December 2022 · Accepted: 7 March 2023 ·

Published Online: 2 August 2023



View Online



Export Citation



CrossMark

Muting Hao (郝苜婷),<sup>a)</sup> and Luca di Mare

## AFFILIATIONS

Oxford Thermo-Fluids Institute, Department of Engineering Science, University Of Oxford, Oxford OX2 0ES, United Kingdom

<sup>a)</sup> Author to whom correspondence should be addressed: [muting.hao@eng.ox.ac.uk](mailto:muting.hao@eng.ox.ac.uk)

## ABSTRACT

The compressible budget terms in the transport equations of Reynolds stresses are examined from the large eddy simulation (LES) result of the film cooling. The capability of LES and the statistical post-processing procedure were first validated. The compressible Reynolds stress budget terms are then analyzed for both fan-shaped and cylindrical cooling films. The balance of all budget terms is shown. The effect of the blowing ratio on each budget term is examined. The mechanisms by which energy is extracted from the mean flow and distributed among the normal Reynolds stresses are highlighted. The sources of anisotropy in the Reynolds stress distributions are examined in detail, and their relation to the flow patterns of the mean and instantaneous flow is explored. The downstream development of the Reynolds stress budgets is studied, and it is shown that the jets of both fan-shaped and cylindrical films can be split into a near field and a far field with different properties. Far downstream of the cooling films, the Reynolds stress budgets near the wall present similarities with the Reynolds stress budgets in a boundary layer, while the Reynolds stress budgets further away from the wall resemble budgets in a free-shear flow. It is shown that the budgets of the Reynolds stress in the three-dimensional wall jets object of this study obey approximate similarity laws. These laws are based on easily obtained integral scales but need to be modified by suitable powers of the distance from the orifice producing the jet.

© 2023 Author(s). All article content, except where otherwise noted, is licensed under a Creative Commons Attribution (CC BY) license (<http://creativecommons.org/licenses/by/4.0/>). <https://doi.org/10.1063/5.0140670>

## I. INTRODUCTION

Cooling has become an indispensable tool for the thermal protection of hot gas turbine components as higher and higher operating temperatures are targeted. However, overusing cooling air means that too much thermodynamic cost is introduced by the cooling film. A good cooling design achieves high effectiveness when the optimal amount of cooling air is selected. Accurate predictions of film cooling flows are thus essential for seeking this optimal condition during gas turbine design.

The interest in the budgets of Reynolds stresses in realistic industrial applications, such as film cooling, is stimulated by the motivation for improving the predictive capability of Reynolds-averaged Navier–Stokes (RANS). Although there are gradually accurate predicting tools using large eddy simulation (LES) and direct numerical simulation (DNS) available in film cooling studies, Reynolds-averaged Navier–Stokes (RANS) methods are still the main choice of simulations by designers when considering their lower computational cost compared with LES and DNS. RANS, however, loses accuracy because they need turbulence models that introduce inaccuracies to the prediction of film cooling performance. As an example, the standard  $k - \varepsilon$

model, even though widely used for film cooling simulations, have issues such as overprediction of the penetration distance into the mainstream (see Ref. 1) and the underprediction of the jet spreading (see Ref. 2). The inaccuracy of turbulence models in RANS partly stems from the base assumption in modeling the Reynolds stress tensor, which is  $\bar{\rho} \tau_{ij} = -\bar{\rho} u_i'' u_j''$ . One of the most commonly used assumptions for the Reynolds stress tensor in RANS is the Boussinesq eddy-viscosity assumption, which determines the Reynolds stress tensor as linearly related to the mean strain-rate tensor ( $\bar{S}_{ij}$ ). Such an assumption is not capable of correctly handling anisotropy and inhomogeneity in flows with rapid variations of mean strain rate and flows with secondary flows. Budgets are one of the criteria for assessing the limitations of available RANS turbulence models. Analyzing related budget terms can also help better understand the physics of turbulence flows.

In the past few years, DNS and LES simulations have been used to provide detailed turbulence statistical quantities including Reynolds stress budgets, turbulent kinetic energy budgets, and other quantities shown in turbulence models. Reynolds stress budgets have been so far studied in flat plates,<sup>3</sup> turbulent boundary layers,<sup>3</sup> channels,<sup>4</sup> pipes,<sup>5</sup>

and interactions between shock waves and turbulent boundary layers.<sup>6</sup> Nicholson *et al.*<sup>7</sup> compared DNS results with results from RANS simulations based on zero-equation, one-equation, two-equation, and eddy-viscosity models in favorable pressure gradient turbulent boundary layers. They found that the reduction of Reynolds stress can be considerably underpredicted under a stronger pressure gradient by all examined RANS models. They illustrated that the Boussinesq assumption leads to underpredicted wall-normal Reynolds stresses but reasonable Reynolds shear stress. Hoyas and Jiménez<sup>8</sup> obtained the Reynolds number effects on the Reynolds-stress budgets in turbulent channels in an incompressible equation. Vyas *et al.*<sup>6</sup> resolved the Reynolds stress budgets in an impinging shock-wave boundary-layer interaction using the compressible equation based on implicit LES results. However, the studies on the compressible version of Reynolds stress budgets are still limited. For film cooling, there have been no studies on budgets of Reynolds stress in the open literature. Only very few studies discussed budgets of turbulent kinetic energy in film cooling. Muldoon and Acharya<sup>9</sup> assessed terms of  $k - \varepsilon$  equations in cooling films by using DNS. They obtained the terms in the  $k - \varepsilon$  equations directly by using DNS and compared them with the same terms calculated by using the standard  $k - \varepsilon$  model. They showed that the eddy viscosity of the standard  $k - \varepsilon$  equations presented a non-negligible error when simulating film cooling. However, they used incompressible Navier–Stokes equations, and they ignored the effect of the compressibility on their budget terms.

Studies on both the LES or DNS of film cooling<sup>10–12</sup> and the budgets of stresses or energy<sup>13–15</sup> have been increasingly pursued recently, and there is so far no study on the Reynolds stress budgets in the film cooling cases.

In a recent turbulence paper by the authors,<sup>16</sup> the downstream evolution of Reynolds stress profiles has been discussed. It is shown that the flow cannot attain similarity at all blowing ratios within 5 diameters downstream of the film. This happens because at a high blowing ratio, the direction of momentum transfer between the film and its surroundings is not uniform. Self-similarity of the mean velocity and temperature defect profiles is attained at a larger distance from the film in the outer parts of the wall jets. The similarity variables are the thickness of the film layer and the velocity defect at half of the film layer thickness. However, the Reynolds stress far downstream only obeys similarity in the first approximation.

The target of the present study is to measure the budget terms in the compressible transport equations of Reynolds stresses based on the LES results of film cooling cases. The budget terms for the fan-shaped hole and the cylindrical hole cases are compared. The effect of the blowing ratio on the budget terms is also discussed. The focus on the budget analysis first expects to provide a dynamic balance of statistical correlations. The Reynolds stress budgets are examined in the near field and in the far field, i.e., in the developing section of the jet and in the self-similar section of the jet.

The sources of anisotropy in the Reynolds stress distributions are examined in detail, and their relation to the flow patterns of the mean and instantaneous flow is explored. Furthermore, the downstream development of the Reynolds stress budgets is studied, and it is shown that the jets of both fan-shaped and cylindrical films can be split into a near field and a far field with different properties, consistent with the observed properties of the Reynolds stress profiles. It is shown that the budgets of the Reynolds stress in the three-dimensional wall jets object

of this study obey approximate similarity laws. These laws are based on easily obtained integral scales but need to be modified by suitable powers of the distance from the orifice producing the jet.

This paper is structured as follows. Section II describes the numerical methodology, and the equations of Reynolds stress budgets in the compressible version of the transport equation. Section IV first recalls some features of the mean and instantaneous flow and then shows the balancing of Reynolds stress budgets; a broad view of the production term of Reynolds stress budgets is studied and its implications for the downstream development of the jets are drawn; self-similarity pattern based on the effect of blowing ratio on Reynolds stress budgets is finally introduced.

## II. METHODOLOGY

### A. Flow conditions and numerical methodology

The flow configuration, including the geometries of the cooling film, the computational domain, and the flow conditions, is selected to match the experiment presented in Gritsch *et al.*<sup>17,18</sup> Based on this, the computations are operated and validated in Hao and di Mare<sup>16</sup> and fully recorded in Hao.<sup>19</sup>

Figure 1 shows the geometries of the two film cooling holes used in this study: the fan-shaped hole and the cylindrical hole. The two cooling holes are inclined at  $30^\circ$ , and they have a length-to-diameter ratio of  $L/D = 6$ , where  $D = 0.01$  is the diameter of the hole. As shown in Fig. 1, the coordinate system is built with the origin at the center of the hole exit plane, the  $x$  axis in the streamwise direction, the  $y$  axis in the wall-normal direction, and the  $z$  axis in the spanwise direction.

Table I lists the operating conditions focused on in the study. Three blowing ratios  $BR = 0.5, 1.0, 1.5$  are especially focused on. Figure 2 presents the computational domain for the two types of cooling holes. The computational domain consists of an external mainstream channel, an internal coolant channel, and a cooling hole connecting the two channels. A near-field region is determined for the region between  $x/D = 1$  and  $x/D = 5$ . A far-field region is determined for the region downstream from  $x/D = 5$ . These two regions are also labeled in Fig. 2 for the following study.

The mesh applied is multiblock hexahedral grids generated by the mesh generator “H4X” which has been validated in Hao *et al.*<sup>20</sup> H4X employs a trunk-and-branch template to build the layout of the cooling film, combined with elliptic smoothing with the grid points on the boundary surfaces sliding while control functions are used to enforce the near-wall grid spacing. Such a mesh can greatly satisfy the

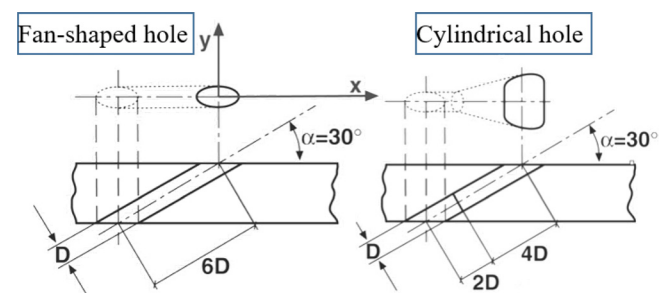


FIG. 1. The geometry of film cooling holes: left (a) fan-shaped hole and right (b) cylindrical hole.<sup>17</sup>

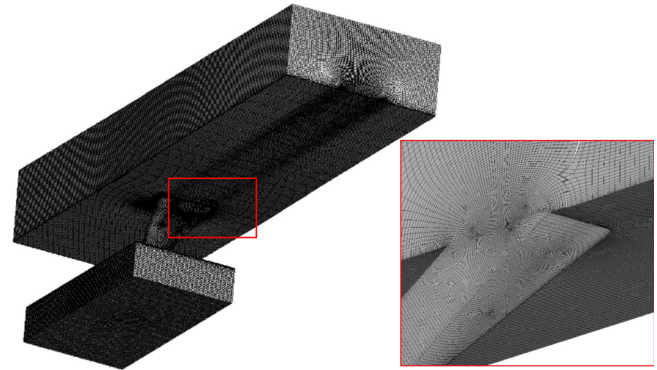
**TABLE I.** Operating conditions of the film-cooling cases.

Parameter	Symbol	Value
Internal temperature	$T_{tc}$	290 K
Blowing ratio	$M$	0.5, 1.0, 1.5
Pressure ratio	$T_{tc}/T_{tm}$	0.54
Internal Mach number	$Ma_c$	0
External Mach number	$Ma_m$	0.6
Internal Reynolds number	$Re_{Dc}$	up to $2.5 \times 10^5$
External Reynolds number	$Re_{Dm}$	up to $1.3 \times 10^5$
Boundary layer thickness	$\delta_{99}/D$	0.5
External turbulence level	$Tu_m/D$	<1.5%
Internal turbulence level	$Tu_c/D$	<1%

grid orthogonality near the surface and smoothness throughout the computational domain. These can be reflected in Fig. 3 which shows the mesh for the fan-shaped case as an example with the mesh on the cutting median section zoomed in. The number of grids is 9674k for the fan-shaped case and 1053k for the cylindrical case.

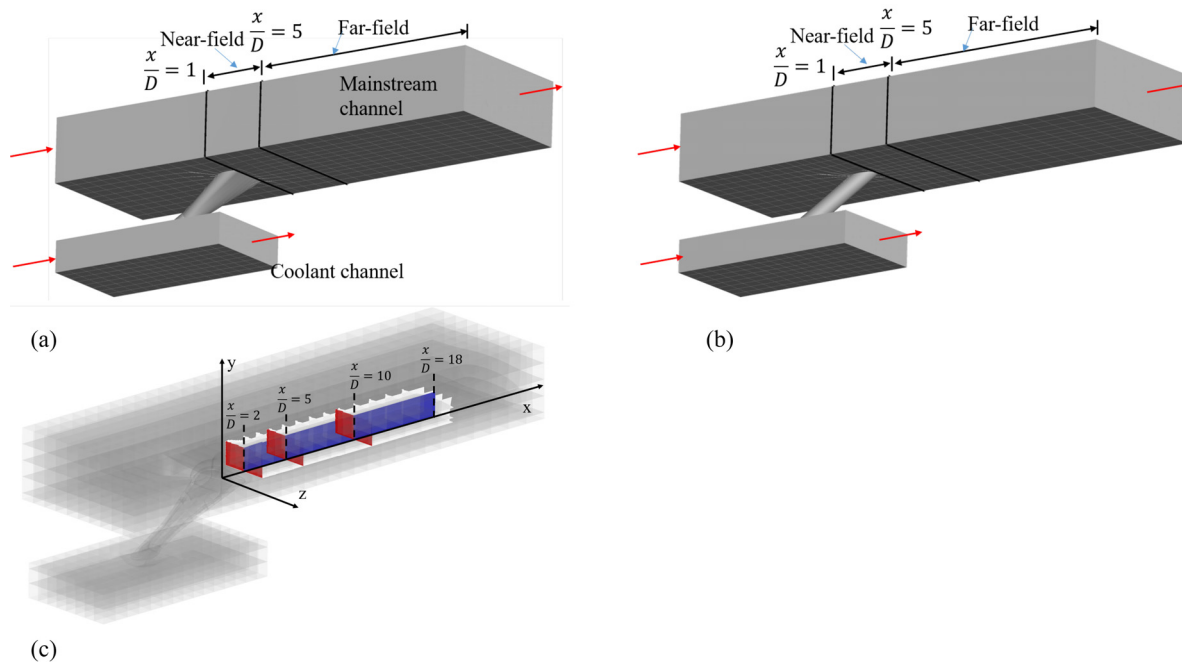
The LES simulations are run by a homegrown CFD code H4X. The code is based on an implicit LES using the finite volume method to solve the conservation laws.

The cell center is used to store variables. On the cell interface, fluxes are evaluated. Flow characteristic variables are extrapolated to the cell interface by a third-order limiter.<sup>21</sup> For obtaining slope limiters, a weight least squares method is used to obtain the gradients. For the inviscid flux, a method of biased stencil is applied, while the Roe

**FIG. 3.** The mesh of the fan-shaped case with the view on the median cutting plane.

Riemann solver is used to evaluate the flux. This leads to a biased three-point stencil and then a third-order scheme away from discontinuities and local extrema. For the viscous flux, the unbiased least squares method is used to evaluate the gradient. As a result, the viscous flux is centered and has second-order accuracy.

The time advancing applies the third-order Runge–Kutta scheme. The Courant number is chosen as 0.8 as the limit, and lower values are adopted during simulations. The boundary conditions are partly shown in Fig. 2 with red arrows indicating the inlet and outlet. The inlet boundary condition is constructed by a synthetic turbulent inflow generator based on eigenmode decomposition.<sup>22</sup> The outlet boundary condition applies the unsteady nonreflecting boundary

**FIG. 2.** (a) Fan-shaped hole computational domains (top left), (b) cylindrical hole computational domains (top right), (c) the key slice (red:  $x/D = 2, 5, 10, 18$ , blue:  $y = 0$ ) and line positions (blue:  $x/D = 2, \dots, 18$ ,  $y = 0$ ) studied in Results and Discussion.

proposed by Thompson.<sup>23</sup> The sidewall of the mainstream channel is applied with the periodic boundary condition. The top wall of the mainstream and the bottom wall of the coolant channel are using far-field boundaries. The rest of the walls are treated with non-slip adiabatic wall boundary conditions. Open multi-processing (OpenMP) and application program interface (API) are implemented for the parallelism of running. 480 processors in parallel are used for LES computations. The complete description of the numerical method, the validation of the meshing, and the validations of the numerical method with LES results are shown in Hao and di Mare.<sup>16</sup>

The Reynolds averages and Favre averages are obtained from statistics of the last 14 flow through times in the unsteady compressible LES results for each case. Namely, around 8000 instantaneous samples are used for the averaging operations.

## B. Equations for Reynolds-average, Favre-average, Reynolds stress budgets

The two forms of averaging this study related to are Reynolds averaging and Favre averaging. For a dependent variable  $f$ , Reynolds-averaging partitions  $f$  into an ensemble mean and a fluctuation. The Reynolds decomposition takes the form

$$f(\mathbf{x}, t) = \bar{f}(\mathbf{x}, t) + f'(\mathbf{x}, t). \quad (1)$$

The Favre average is defined as

$$\tilde{f} = \frac{\bar{\rho f}}{\bar{\rho}}. \quad (2)$$

The Favre-averaging procedure partitions  $f$  into the Favre average and a fluctuation. The Favre decomposition consequently reads

$$f(\mathbf{x}, t) = \tilde{f}(\mathbf{x}, t) + f''(\mathbf{x}, t). \quad (3)$$

The Favre-averaged Reynolds-stress tensor is

$$\bar{\rho} \tau_{ij} = -\overline{\rho u_i'' u_j''}. \quad (4)$$

The transport equation of the Reynolds-stress tensor in the compressible situation is obtained in a way that the dependent variables take the Favre-averaged form while the equations are in the Reynolds-averaged form. The derivation is achieved by adding two Reynolds-averaged equations, one of which is the product of  $u_i''$  with the fluctuating momentum equation for  $u_j''$ , and the other is the product of  $u_j''$  with the fluctuating momentum equation for  $u_i''$ . The transport equation of the stress tensor can be written in the form<sup>24</sup>

$$\begin{aligned} \bar{\rho} \frac{D\tau_{ij}}{Dt} &= \frac{\partial(\bar{\rho} \tau_{ij})}{\partial t} + \frac{\partial}{\partial x_k} (\tilde{u}_k \bar{\rho} \tau_{ij}) \\ &= \bar{\rho} P_{ij} + \bar{\rho} \Pi_{ij} - \bar{\rho} \varepsilon_{ij} + \bar{\rho} M_{ij} + \bar{\rho} D_{ij}, \end{aligned} \quad (5)$$

where

$$\text{production} \quad \bar{\rho} P_{ij} = -\bar{\rho} \left[ \tau_{ik} \frac{\partial \tilde{u}_j}{\partial x_k} + \frac{\partial \tilde{u}_i}{\partial x_k} \tau_{kj} \right], \quad (6)$$

$$\text{redistribution} \quad \bar{\rho} \Pi_{ij} = \overline{p' \left( \frac{\partial u_i''}{\partial x_j} + \frac{\partial u_j''}{\partial x_i} \right)} = \overline{p' \left( \frac{\partial u_i'}{\partial x_j} + \frac{\partial u_j'}{\partial x_i} \right)}, \quad (7)$$

$$\text{dissipation} \quad \bar{\rho} \varepsilon_{ij} = \overline{\sigma_{ik}'' \frac{\partial u_j''}{\partial x_k}} + \overline{\sigma_{jk}'' \frac{\partial u_i''}{\partial x_k}} = \overline{\sigma_{ik}' \frac{\partial u_j'}{\partial x_k}} + \overline{\sigma_{jk}' \frac{\partial u_i'}{\partial x_k}}, \quad (8)$$

mass flux contribution

$$\begin{aligned} \bar{\rho} M_{ij} &= \overline{\rho' u_i'' \left( \frac{\partial \bar{p}}{\partial x_j} - \frac{\partial \bar{\sigma}_{jk}}{\partial x_k} \right)} + \overline{\rho' u_j'' \left( \frac{\partial \bar{p}}{\partial x_i} - \frac{\partial \bar{\sigma}_{ik}}{\partial x_k} \right)} \\ &= \overline{\rho' u_i' \left( \frac{\partial \bar{p}}{\partial x_j} - \frac{\partial \bar{\sigma}_{jk}}{\partial x_k} \right)} + \overline{\rho' u_j' \left( \frac{\partial \bar{p}}{\partial x_i} - \frac{\partial \bar{\sigma}_{ik}}{\partial x_k} \right)}, \end{aligned} \quad (9)$$

$$\text{diffusion} \quad \bar{\rho} \mathcal{D}_{ij} = \bar{\rho} \mathcal{D}_{ij}^v + \bar{\rho} \mathcal{D}_{ij}^T + \bar{\rho} \mathcal{D}_{ij}^p, \quad (10)$$

$$\begin{aligned} \text{viscous diffusion} \quad \bar{\rho} \mathcal{D}_{ij}^v &= \frac{\partial}{\partial x_k} \left( \overline{\sigma_{ik}'' u_j''} + \overline{\sigma_{jk}'' u_i''} \right) \\ &= \frac{\partial}{\partial x_k} \left( \overline{\sigma_{ik}' u_j'} + \overline{\sigma_{jk}' u_i'} \right), \end{aligned} \quad (11)$$

$$\begin{aligned} \text{turbulent diffusion} \quad \bar{\rho} \mathcal{D}_{ij}^T &= -\frac{\partial}{\partial x_k} \left[ \overline{\rho u_i'' u_j'' u_k''} \right] \\ &= -\frac{\partial}{\partial x_k} \left[ \overline{\rho u_i' u_j' u_k'} \right], \end{aligned} \quad (12)$$

$$\begin{aligned} \text{pressure diffusion} \quad \bar{\rho} \mathcal{D}_{ij}^p &= -\frac{\partial}{\partial x_k} \left[ \overline{\delta_{ik} p' u_j'} + \overline{p' u_i' \delta_{jk}} \right] \\ &= -\frac{\partial}{\partial x_k} \left[ \overline{\delta_{ik} p' u_j'} + \overline{p' u_i' \delta_{jk}} \right], \end{aligned} \quad (13)$$

where  $\sigma_{ij}$  is the viscous stress tensor for a Newtonian fluid, with  $\mu$  as the shear viscosity, and  $\delta_{ij}$  as the Kronecker delta

$$\sigma_{ij} = 2\mu \left( S_{ij} - \frac{\delta_{ij}}{3} S_{kk} \right) \quad (14)$$

based on strain-rate tensor  $S_{kl}$ , which takes the following form:

$$S_{kl} = \frac{1}{2} \left( \frac{\partial u_k}{\partial x_l} + \frac{\partial u_l}{\partial x_k} \right). \quad (15)$$

The transport of the Reynolds stress shown in Eq. (5) is balanced among its production term, redistribution (pressure strain) term, dissipation term (resolved viscous dissipation), mass flux contribution, and diffusion terms. Diffusion terms are comprised of viscous diffusion (or molecular diffusion), turbulent diffusion (or turbulent transport), and pressure diffusion. An exhaustive overview of compressible turbulence budget is given in the book by Gatsk and Bonnet.<sup>24</sup>

## III. VALIDATION

The LES procedure used in this paper has been validated by comparing computed flowfield and heat transfer characteristics with experimental data in a recent paper<sup>16</sup> by the authors. The results in this section focus on the validity of the procedure to compute terms in the Reynolds stress budget.

The correctness of the Reynolds-stress budget algorithm is validated in Spalart's  $Re_\tau = 670$  turbulent boundary layer case.<sup>25</sup> The incompressible version of Reynolds-stress budget terms is used in this case according to Spalart.<sup>25</sup> The Reynolds stress budgets computed using the authors' LES code are compared with the results from the DNS data in Spalart,<sup>25</sup> as shown in Fig. 4.

Figure 4 presents the comparison of the production, the turbulent diffusion, the viscous diffusion, the dissipation, and the pressure-velocity correlation budget terms in the incompressible transport

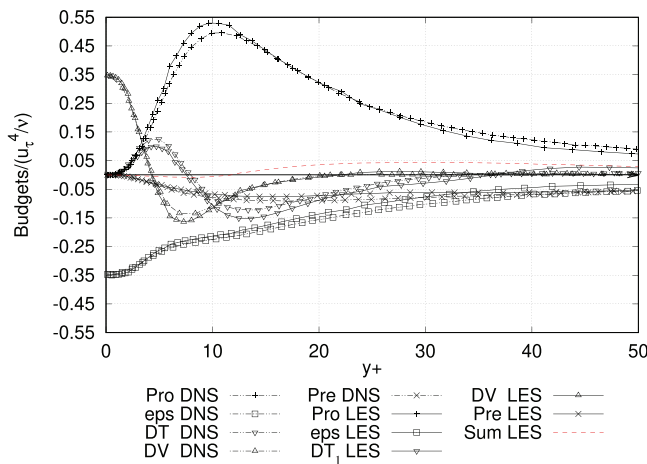


FIG. 4. Budget terms of  $\widetilde{u''u''}$  for Spalart's turbulent boundary layer.<sup>25</sup>

equation of the Reynolds stress. The scaling  $u_\tau^4/\nu$  adopted in this case is the same as Spalart's<sup>25</sup> paper. An imbalance expressed in the following equation is also shown (in red dashed line), indicating the error in the solution:

$$\text{imbalance} = \bar{\rho} P_{ij} + \bar{\rho} \Pi_{ij} - \bar{\rho} \varepsilon_{ij} + \bar{\rho} M_{ij} + \bar{\rho} D_{ij} - \frac{\partial}{\partial x_k} (\widetilde{u_k \bar{\rho} \tau_{ij}}). \quad (16)$$

Equation (16) is obtained by subtracting the left-hand side of Eq. (5) and ignoring the time-derivative term. When using LES, the imbalance is a measure of the effect of subgrid scale (SGS) on the resolved budgets as well as the effect brought by ignoring the time-derivative term, plus unresolved dissipation. The budget generated from the present LES result matches well with the DNS data in both the viscous layer and log-law region. The maximum imbalance is observed at around  $y^+ = 25$ , with a deviation of less than 0.05 at maximum, which is smaller than the budget error using LES in Vyas *et al.*<sup>6</sup>

Above all, both the cooling film LES results and the procedure generating the Reynolds stress budget terms can be considered trustworthy.

## IV. RESULTS AND DISCUSSION

### A. Structure of the flow mean and instantaneous flow field

Before addressing the structure of the Reynolds stress budgets on the center plane of the flow, it is useful to recall some qualitative features of the mean and instantaneous flow fields. Sections of the flow field at  $x/D = 2, 5, 10$  for the fan-shaped film are shown in Fig. 5, while the positions of these slices are shown in Fig. 2(c). The mean flow is shown through contours of the stream-wise velocity component and vectors of the velocities tangential to planes at constant  $x$ . The wall jet issuing from the fan-shaped film stays confined in a layer of a modest thickness (comparable to the film diameter) and spreads gradually outwards. As a consequence, the coolant is drawn further toward the wall and outwards as it mixes with the hot stream. The instantaneous contours of streamwise vorticity similarly show a weakly

localized set of turbulence structures located in the lower half of the jet and not much stronger than the surrounding boundary layer turbulence.

The development of the wall jet produced by a cylindrical film is shown in Fig. 6. The situation here is considerably different because the jet is confined on the sides by a pair of counter-rotating vortices. The vortices induce a positive wall-normal velocity on the center plane which lifts coolant away from the wall and favors a rapid mixing of the coolant with the hot stream. The fluid is entrained back into the space between the vortices and the wall on the edge of the jet. Turbulent motion is particularly intense in the area immediately downstream of the film ( $x/D = 2$ ) and gradually dies out further downstream. The area downstream of the film is remarkable because of its anisotropy, as it will be shown in Sec. IV B. Anisotropy is promoted by the proximity of the wall and of the jet and causes the span-wise velocity fluctuations to be more intense than the other two components. Eddies from the hot mainstream slide under the jet alternatively from the left and the right.

### B. General balancing of budget terms

The budgets of  $\widetilde{u''u''}$ ,  $\widetilde{v''v''}$ ,  $\widetilde{w''w''}$ , and  $\widetilde{u''v''}$  downstream the film cooling holes of two types are shown in Figs. 7, 8, 9, and 10, respectively, with the position shown as black dash lines in Fig. 2. A two-layer structure in the Reynolds stress budgets is observed which is similar to the one found in the Reynolds stress in Ref. 16. The patterns of Reynolds stresses and corresponding budget terms can be categorized into two regions. One region is near the wall where the general features of the flow resemble a developing boundary layer. Another region is across the jet where the general features of the flow resemble a shear layer.

In Figs. 7–10, the budget terms are rescaled using the scaling factor

$$\frac{\Delta u^3}{\delta_{99}} \left( \frac{x}{D} \right)^{-\beta}, \quad (17)$$

where  $\delta_{99}$  is the height when the velocity arrives at 99% of the free-stream velocity,  $\Delta U$  is the Favre-averaged velocity defect, and  $\beta$  is the exponent factor. The method of obtaining  $\delta_{99}$  and  $\Delta U$  is shown in Fig. 11(a). The value chosen for  $\beta$  depends on the geometry of the film, but not on the blowing ratios.  $\beta = 0.5$  is adopted for the fan-shaped films and  $\beta = 0.9$  is adopted for the cylindrical films. The reason for choosing these values is explained in Sec. V.

#### 1. $\widetilde{u''u''}$ budget

In fan-shaped cooling films [shown in Fig. 7(a)], the main source of  $\widetilde{u''u''}$  is the production term [shown in Eq. (6)] throughout the thickness of the jet layer and the boundary layer. The main sink is the redistribution term [shown in Eq. (7)] away from the wall, whereas near the wall it is the dissipation [shown in Eq. (8)]. The convection immediately downstream the film takes energy from the core of the jet to the jet edge and toward the wall. This is because the jet between  $y/\delta_{99} = 0.2 - 0.4$  is diffusing. The convection by the mean flow moves fluid toward the wall and spreads it outwards, as indicated in Sec. IV A. The turbulent diffusion [shown in Eq. (12)] transfers energy from the local maximum of Reynolds stresses near the wall and near

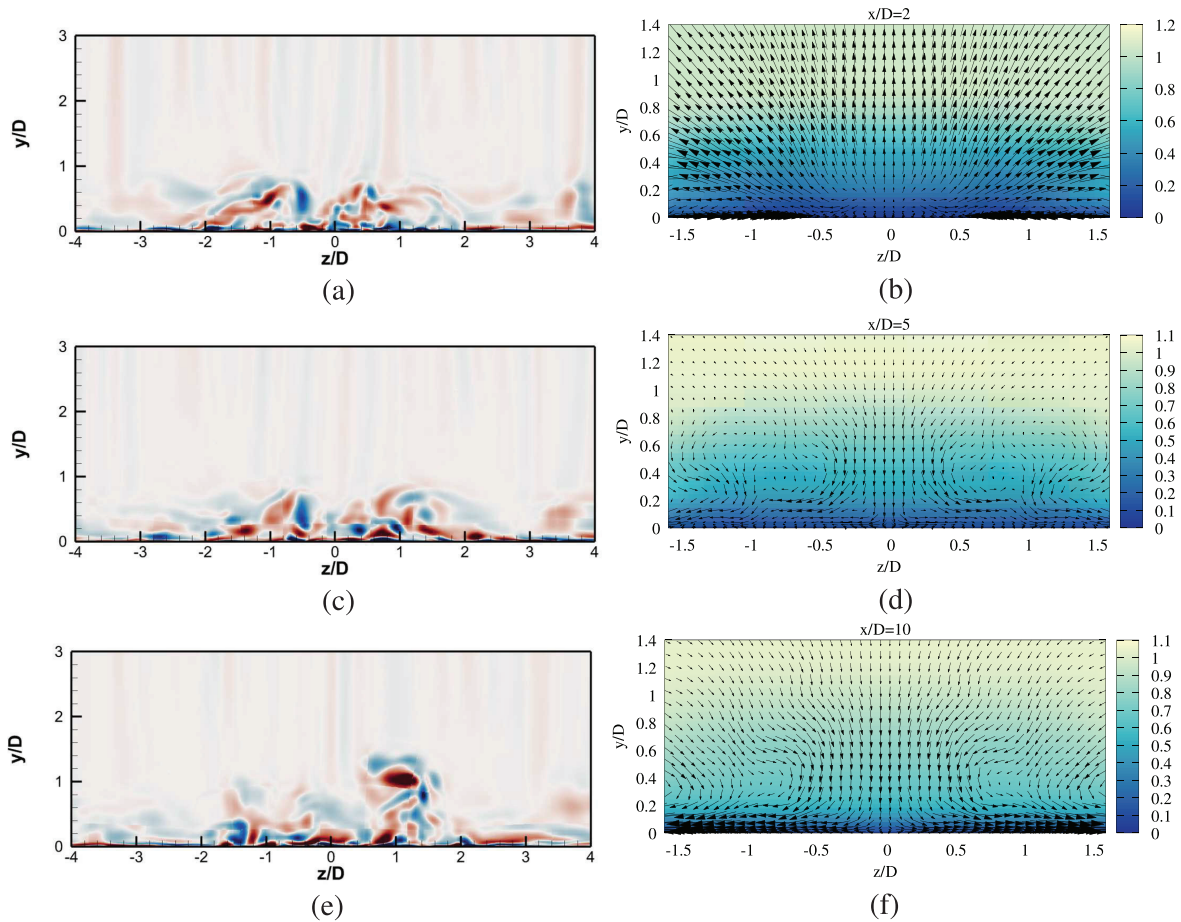


**FIG. 5.** Contours of instantaneous streamwise vorticity (left) and mean streamwise velocity with mean velocity vectors (right) for fan-shaped films at  $x/D = 2$ ,  $x/D = 5$ , and  $x/D = 10$ , at  $Br = 1.0$ : (a) instantaneous  $w_x$ ,  $x/D = 2$ , (b)  $U$  contours and vectors of  $(w, v)$ ,  $x/D = 2$ , (c) instantaneous  $w_x$ ,  $x/D = 5$ , (d)  $U$  contours and vectors of  $(w, v)$ ,  $x/D = 5$ , (e) instantaneous  $w_x$ ,  $x/D = 10$ , and (f)  $U$  contours and vectors of  $(w, v)$ ,  $x/D = 10$ .

the core of the jet to the edge of the jet and toward the wall, and also toward the region between the core and the wall. The pressure diffusion [shown in Eq. (13)] has two sources, in the proximity of the wall and just below the core of the jet, and two sinks, at the bottom of the Reynolds stress and the top of the jet. The mass flux term [shown in Eq. (9)] is generally very small, except in the proximity of the outlet of the cooling hole. It acts as a sink at the core of the jet.

As the flow travels downstream, the amplitudes of the major sources and sinks away from the wall are preserved by the scaling, shown in Eq. (17). Meanwhile, the amplitudes of the major source and sink terms near the wall grow significantly with the respect to the outer scaling. When the flow arrives  $x/D = 10$ , the convection and the turbulent diffusion account for a larger proportion of the source and sink far away from the wall. At  $y/\delta_{99} = 0.2 - 0.7$ , the convection behaves as the source, whereas the turbulent diffusion behaves as the sink. At  $y/\delta_{99} = 0.7 - 1.0$ , both of these two terms switch their roles as the source and the sink. At  $y/\delta_{99} = 0.2 - 1.0$ , the production and the redistribution accounted for a smaller proportion of budgets whilst retaining the magnitude of the largest terms. In this sense, the total amplitude of the major sources and sinks far from the wall maintain.

Figure 7(b) shows the budgets of  $\widetilde{u''u''}$  in the cylindrical cooling film. In Fig. 7(b), the production is still the major source of  $\widetilde{u''u''}$ . Compared with the fan-shaped cooling film case, there is a unique feature at  $x/D = 2$ : apart from the peak in the wall layer, there are two other peaks of production away from the wall, which is an inner peak at  $y/\delta_{99} = 0.3$  and an outer peak at  $y/\delta = 0.8$ . This corresponds to the shape of the Reynolds stress  $u''u''$ . The peak at around  $y/\delta_{99} = 0.3$  is caused by the large flow fluctuations immediately downstream the film described in Sec. IV A. The peak at  $y/\delta_{99} = 0.7$  is caused by the turbulence at the edge of the jet. The local minimum between these two peaks corresponds to an area of low turbulence intensity in the jet as it emerges from the film. The inner peak of production is balanced by redistribution and turbulent diffusion. For the outer peak, production is balanced in equal measure by convection, dissipation, and redistribution. The level of  $u''u''$  at the local minimum at  $y/\delta = 0.5$  between the two peaks is sustained in equal measure by production and turbulent diffusion. The main loss terms are convection and redistribution. There is a region of high turbulent intensity in the proximity of the wall. It is sustained by a sharp peak in the production, balanced by viscous terms of nearly the same amplitude. Between

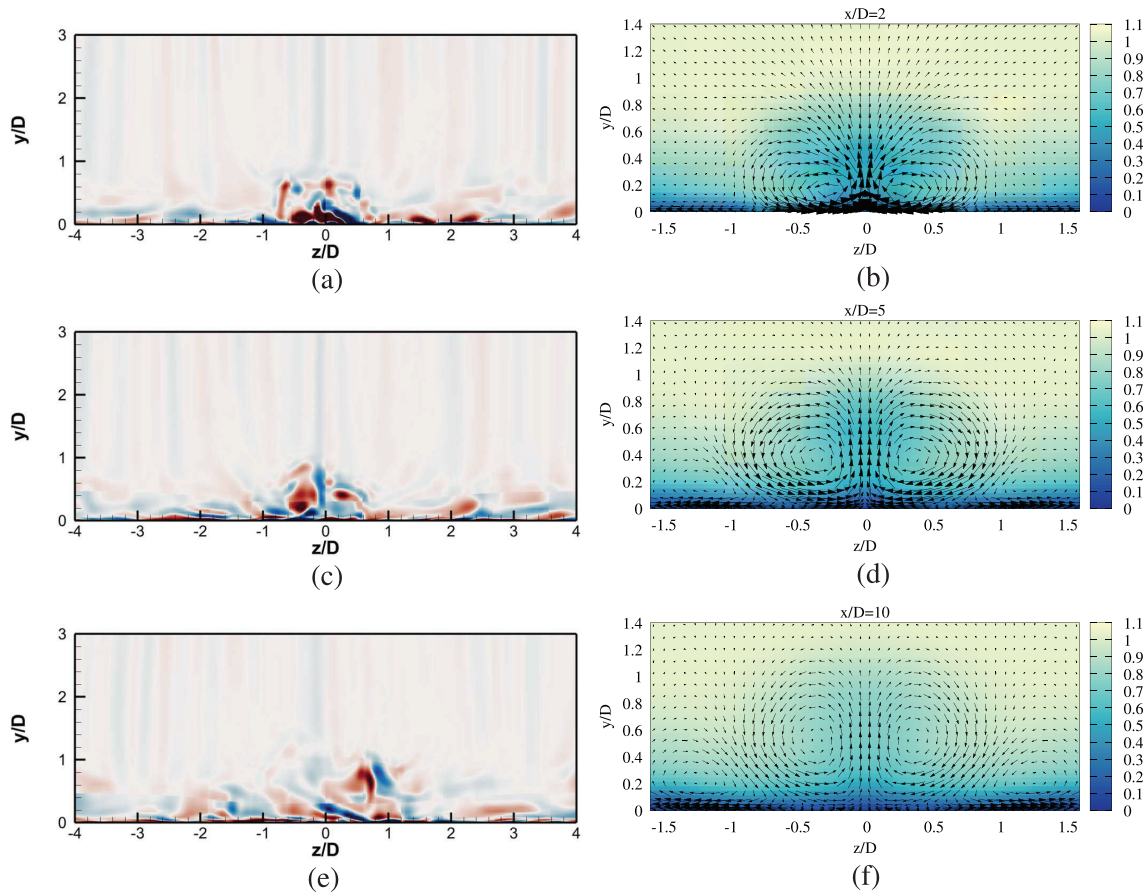


**FIG. 6.** Contours of instantaneous streamwise vorticity (left) and mean streamwise velocity with mean velocity vectors (right) for cylindrical films at  $x/D = 2$ ,  $x/D = 5$  and  $x/D = 10$ , at  $BR = 1.0$ : (a) instantaneous  $w_x$ ,  $x/D = 2$ , (b)  $U$  contours and vectors of  $(w, v)$ ,  $x/D = 2$ , (c) instantaneous  $w_x$ ,  $x/D = 5$ , (d)  $U$  contours and vectors of  $(w, v)$ ,  $x/D = 5$ , (e) instantaneous  $w_x$ ,  $x/D = 10$ , and (f)  $U$  contours and vectors of  $(w, v)$ ,  $x/D = 10$ .

the inner peak and the wall region, turbulence is sustained mainly by convection and redistribution. The budget of  $\overline{u''u''}$  below  $y/\delta_{99} \approx 0.3$  is closed by the viscous terms.

When the jet goes downstream to  $x/D = 5$ , the outer peak of the production continues to be the main source term around the edge of the jet, while the inner peak disappears. This corresponds to the pattern shown in Fig. 6(a): at  $BR = 1.0$ , there is a region confined in the wall-normal direction by the wall and by the lower side of the jet. This region is also confined in the streamwise direction by the lower side of the jet, see Sec. IV A. This is highlighted by the high level of streamwise vorticity fluctuations in Fig. 6(a). At  $x/D = 5$ , the confinement provided by the jet disappears, because the jet becomes nearly horizontal and gradually mixes with the freestream. Therefore, the Reynolds stresses become more nearly isotropic. This causes the inner peak of the production term of  $\overline{u''u''}$  to disappear. Both the redistribution and the convection become the major sink terms far away from the wall. The dissipation maintains the sink near the wall.

When it comes to  $x/D = 10$ , the production maintains the peak of the source. The turbulent diffusion far from the wall becomes the equally major sink together with the redistribution, balancing the peak

of the production. The turbulent diffusion at  $x/D = 0.1 - 0.4$  grows to the main source, which is balanced by the redistribution and dissipation. The reason why turbulent diffusion behaves as a source below  $y/\delta_{99} = 0.4$  and as a sink above  $y/\delta_{99} = 0.4$  is that the flow tries to bring the energy from the peak of Reynolds stress  $\overline{u''u''}$  at  $y/\delta_{99} = 0.7$  to around.

## 2. $\overline{v''v''}$ budget

In Fig. 8(a), the main source of  $\overline{v''v''}$  in the jet layer is the redistribution [shown in Eq. (7)]. In the wall layer,  $\overline{v''v''}$  is sustained mainly by pressure diffusion [shown in Eq. (13)]. The main sink of  $\overline{v''v''}$  is the dissipation [shown in Eq. (8)] in the jet layer, while the main sink of  $\overline{v''v''}$  near the wall is the pressure redistribution. The convection immediately downstream of the hole takes energy from the region around the core of the jet and the top of the jet to the core of the jet and toward the wall. The production immediately downstream of the hole acts as a sink at the core of the jet. Turbulent diffusion transfers energy to the top of the jet and toward the wall. The pressure diffusion has two sources and two sinks. The energy is taken from the region between the near-wall boundary layer and the jet as well as the top

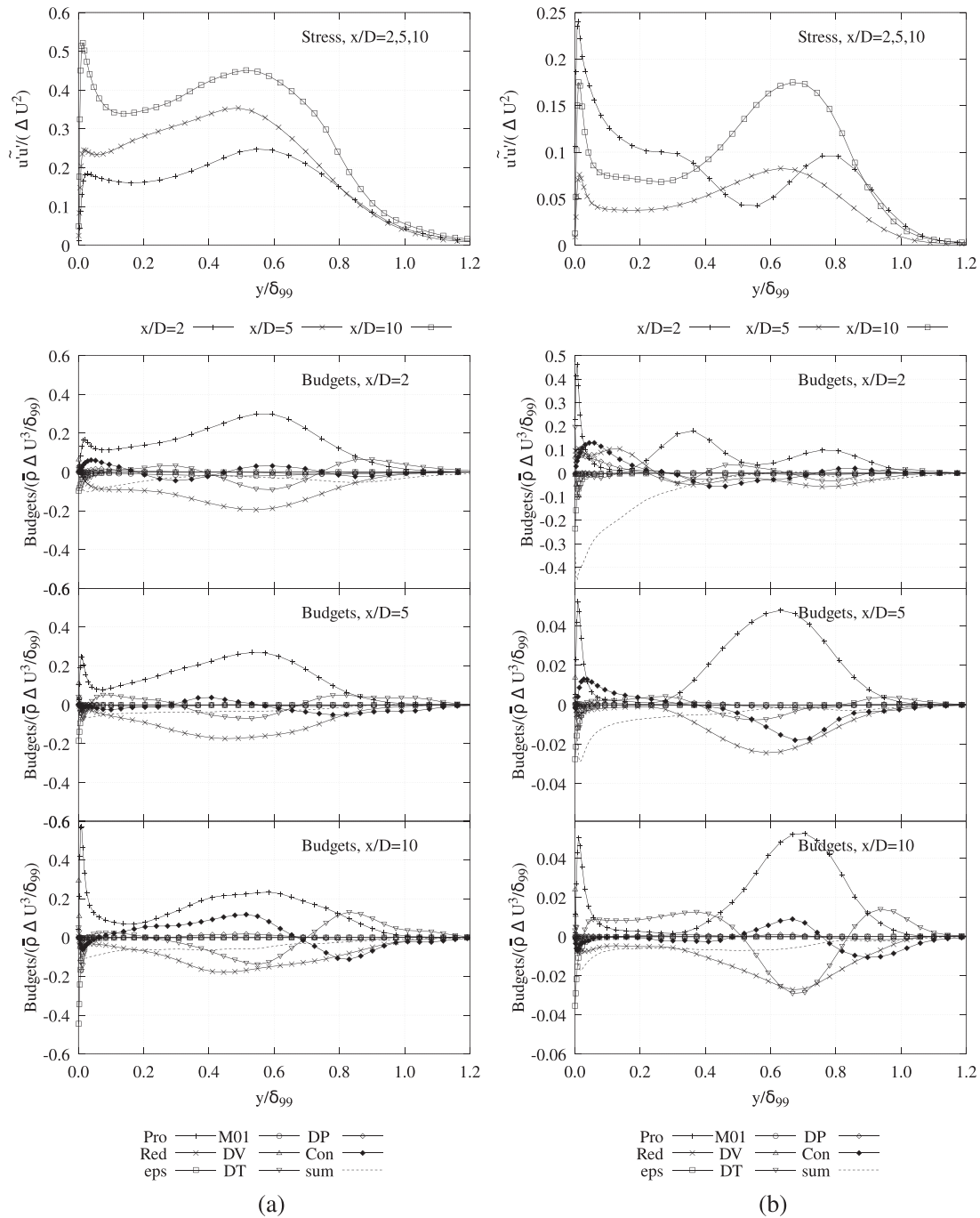


FIG. 7. Reynolds stress  $\overline{u''u''}$  and multiple budget terms on  $\overline{u''u''}$  scaled by  $\Delta U^3 / \delta_{99}$  for fan-shaped and cylindrical films at  $BR = 1.0$ : (a) fan-shaped hole and (b) cylindrical hole.

edge of the jet toward the jet and to the core of the jet. The mass flux term has one source, at the core of the jet, and one sink, slightly above the wall.

At  $x/D = 5$  and  $x/D = 10$ , the redistribution far from the wall is still the main source. It is balanced by turbulent diffusion,

convection, dissipation, and pressure diffusion. Turbulent diffusion behaves as a source beyond the outer edge of the jet.

The main source near the wall is pressure diffusion, which is balanced by the redistribution term. Both of them have a larger amplitude than at  $x/D = 2$ .

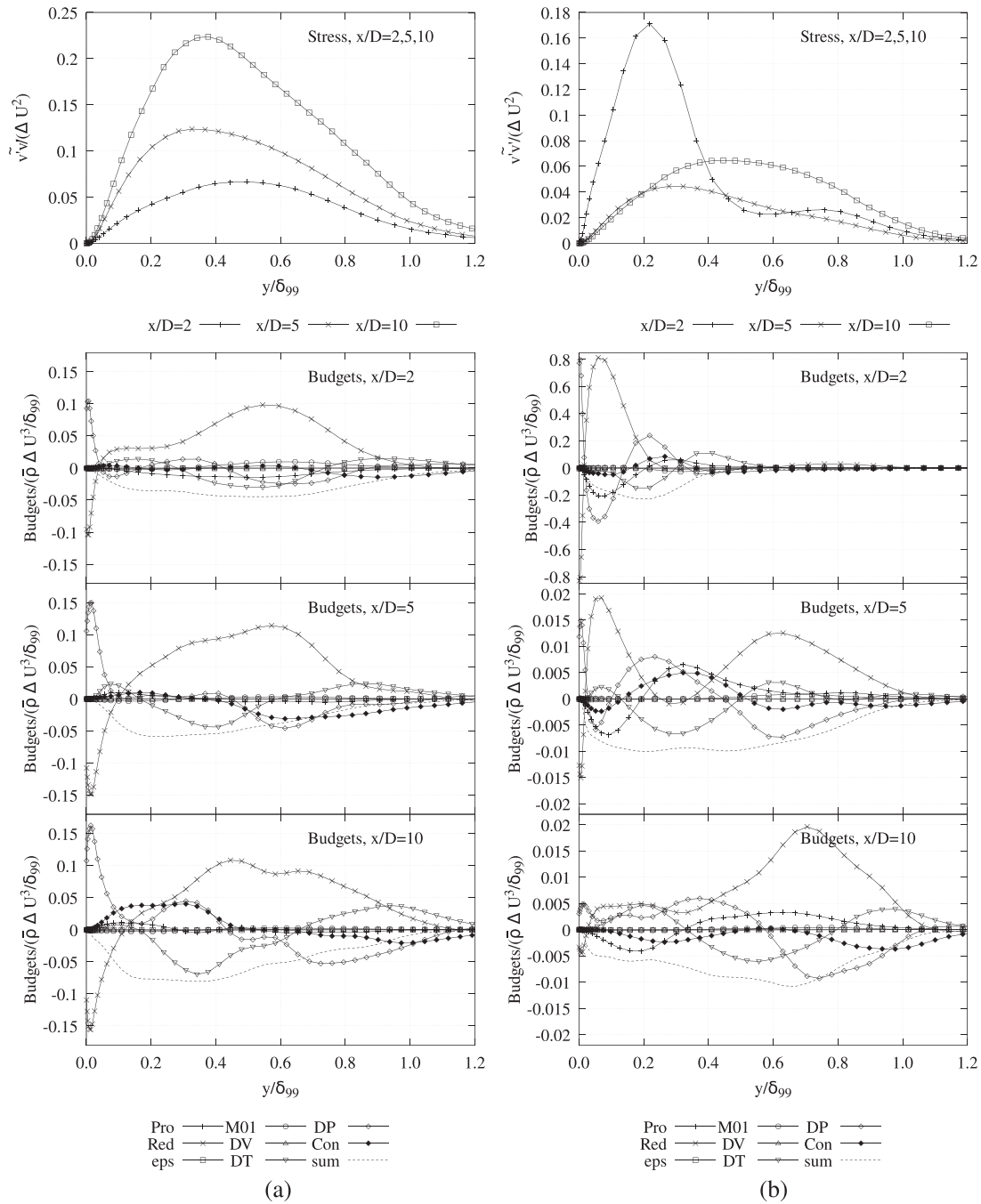


**FIG. 8.** Reynolds stress  $\widetilde{v''v''}$  and multiple budget terms on  $\widetilde{v''v''}$  scaled by  $\Delta U^3/\delta_{99}$  for fan-shaped and cylindrical films at  $BR = 1.0$ : (a) fan-shaped hole and (b) cylindrical hole.

In Fig. 8(b), the budget of  $\widetilde{v''v''}$  at  $x/D = 2$  is dominated by the flow configuration described in the explanation for the budgets of  $u''u''$ , see Sec. IV A. The flow arrangement results in pronounced peaks in the  $v''v''$  and  $w''w''$  Reynolds stresses immediately below the jet corresponding to a flat area in the  $u''u''$  stress. All three

Reynolds normal stress terms are depressed in the area corresponding to the core of the jet itself. In this region, the budget of the wall-normal fluctuations is dominated by pressure redistribution, which acts as the main source below  $y/\delta_{99} = 0.2$ . Here, the main loss terms are pressure diffusion and production. Turbulent diffusion acts as

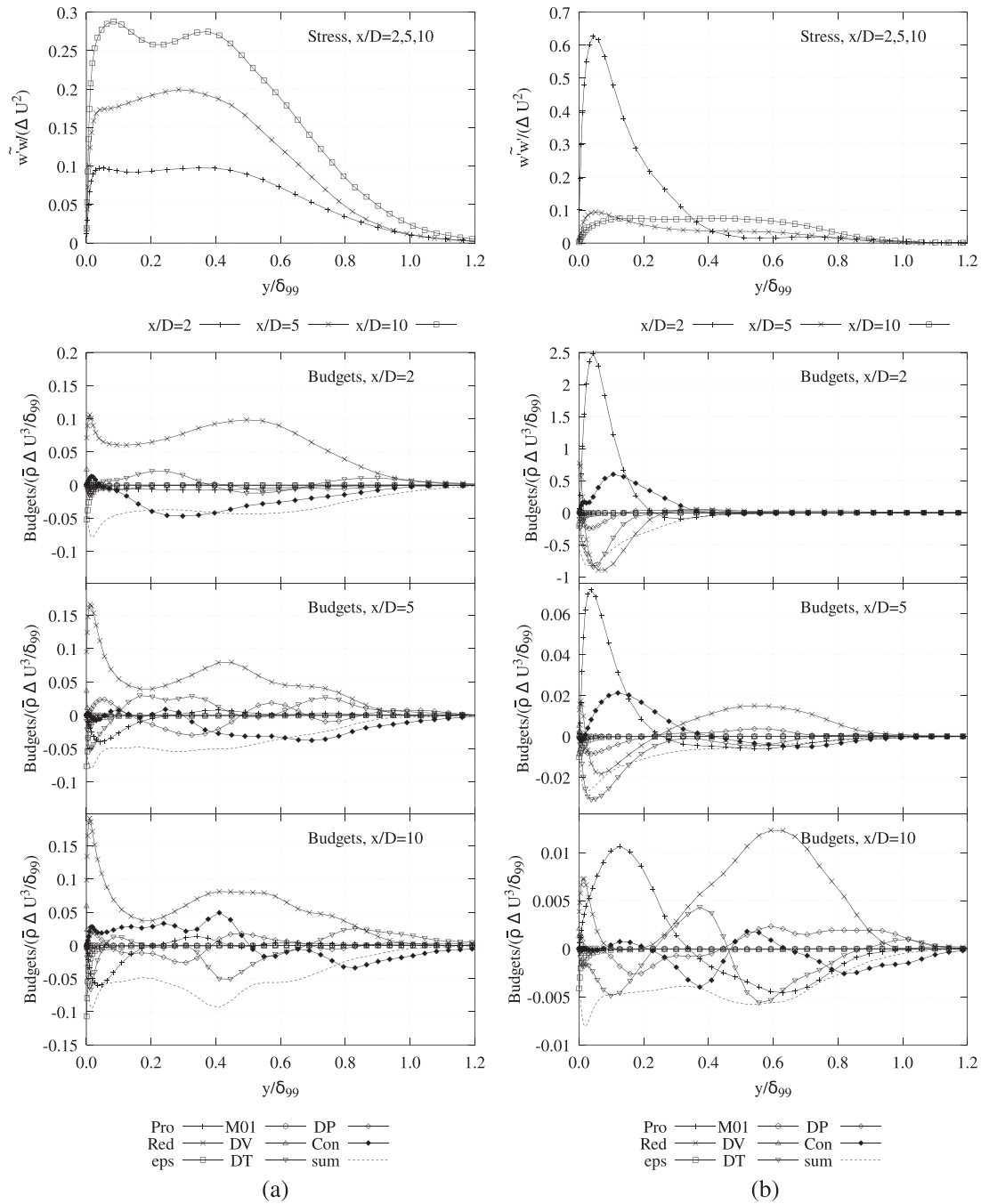


**FIG. 9.** Reynolds stress  $\tilde{w''w''}$  and multiple budget terms on  $\tilde{w''w''}$  scaled by  $\Delta U^3/\delta_{99}$  for fan-shaped and cylindrical films at  $BR = 1.0$ : (a) fan-shaped hole and (b) cylindrical hole.

usual as a sink in areas of high intensity and as a source in areas of low intensity.

The other main sources of the Reynolds stress  $\tilde{v''v''}$  are the convection, production, and pressure diffusion in the area between  $y/\delta_{99} = 0.2$  and  $y/\delta_{99} = 0.4$ . The main sinks are viscous dissipation,

the pressure diffusion (in the outer part of the jet). The turbulent diffusion acts to transfer energy away from the peak at  $y/\delta_{99} = 0.3$  and toward the wall or toward the edge of the jet. Further downstream after  $x/D = 5$ , the distribution of  $v''v''$  becomes flatter. The pressure redistribution is still the main source in the outer part of the jet. The

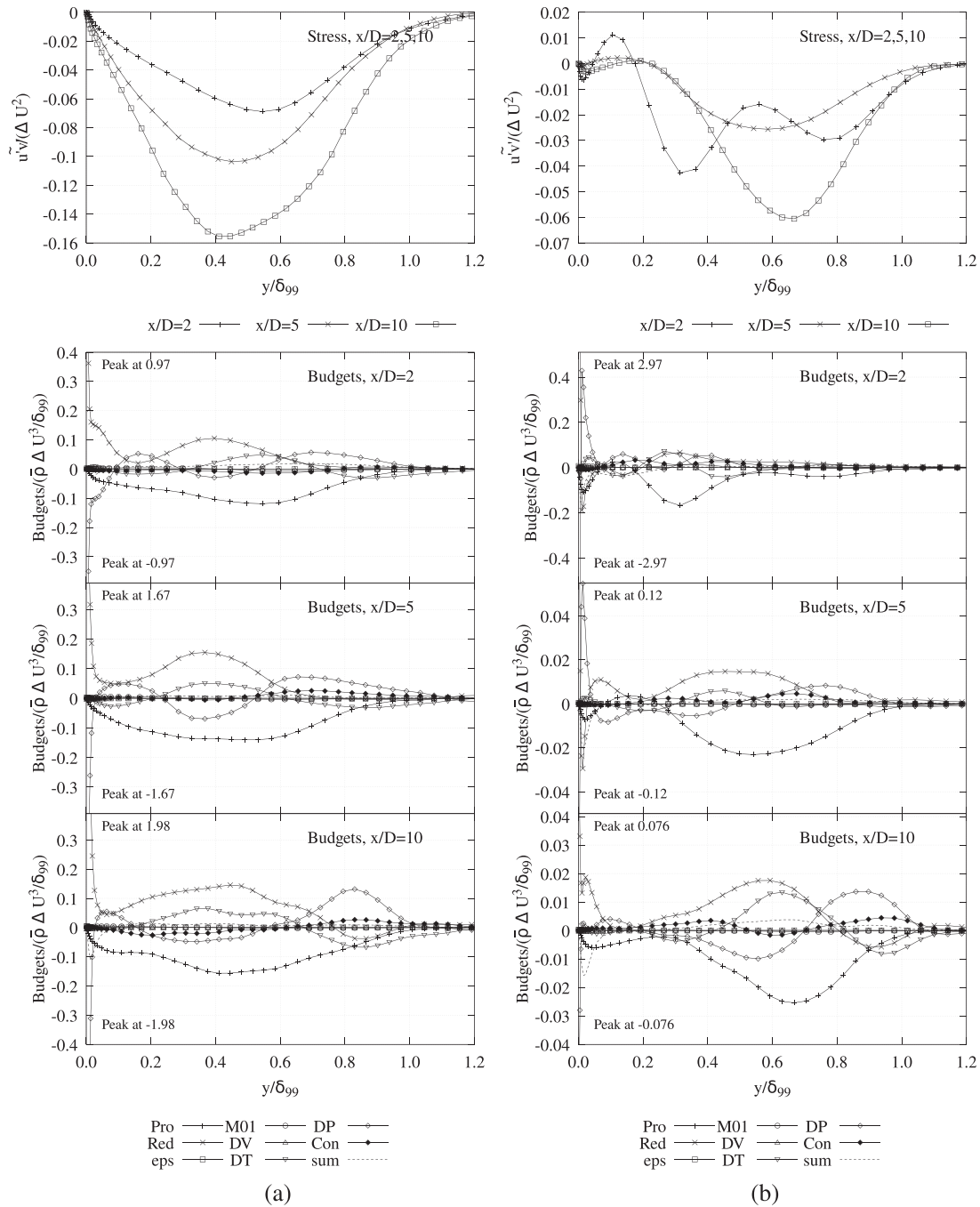


**FIG. 10.** Reynolds stress  $\tilde{u''v''}$  and multiple budget terms on  $\tilde{u''v''}$  scaled by  $\Delta U^3/\delta_{99}$  for fan-shaped and cylindrical films at  $BR = 1.0$ : (a) fan-shaped hole and (b) cylindrical hole.

arrangement of the flow described in Sec. IV A evolves further and the confinement provided by the jet disappears, partly because of the change in the direction of the jet and partly because of its gradual mixing with the surrounding fluid, as mentioned in Sec. IV A. As a result, the amplitude of the peak in the pressure redistribution below  $y/\delta_{99} = 0.2$  is considerably reduced, and its amplitude becomes

comparable to the magnitude of the largest pressure redistribution in the region at the outer edge of the jet ( $y/\delta_{99} \approx 0.6$ ). Production makes a small contribution to the budget of  $v''v''$  around  $y/\delta_{99} \approx 0.4$  at  $x/D = 5$ , and around  $y/\delta_{99} \approx 0.6$  at  $x/D = 10$ . Away from the wall, pressure redistribution and production are balanced by pressure diffusion, convection, and dissipation. The turbulent diffusion moves

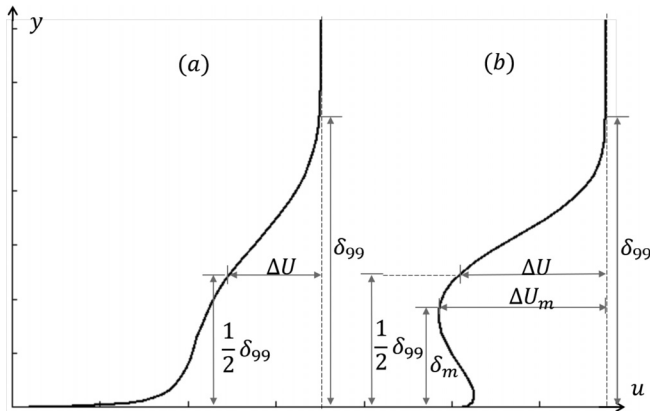


**FIG. 11.** Two types of velocity profiles: (a) for films with attached flow and (b) for films with lifted flow.

energy away from the broad peak at  $y/\delta_{99} = 0.4$  toward the periphery of the jet.

### 3. $\widetilde{w''w''}$ budget

In Fig. 9(a), the main source of  $\widetilde{w''w''}$  both in the jet layer and near the wall is the redistribution, and the main sink is dissipation. The convection immediately downstream (at  $x/D = 2$ ) the hole takes

energy from the wall to the core of the jet. Away from the hole exit (at  $x/D = 5, 10$ ), energy is taken from the region between the wall and the top of the jet to the core of the jet and toward the wall. The production immediately downstream of the hole has one sink and one source. Energy is transferred to the region beneath the jet toward the wall and to the core of the jet. The turbulent diffusion gradually takes the energy from the core of the jet to its periphery. The pressure diffusion has two sources and two sinks. The energy is taken from the near-wall region and the core of the jet to the region between them and to the edge of the jet. The mass flux term of  $\widetilde{w''w''}$  is much smaller and of a lower order of values than the mass flux term of  $\widetilde{u''u''}$  and  $\widetilde{v''v''}$ .

In Fig. 9(b), the budgets of  $\widetilde{w''w''}$  for the cylindrical film immediately downstream of the film are entirely dominated by the large spanwise fluctuations described in Sec. IV A. Closed to the cooling hole, the fluctuations in eddies confined between the jet and the wall give rise to very large production levels below  $y/\delta_{99} = 0.2$ . These high production levels are the direct result of the unsteady flow pattern and become manifested in the  $\widetilde{w''w''}$  budget through the component  $\widetilde{w''w''} \frac{\partial w}{\partial z}$  of the budget term. The energy transferred to the turbulent motion through the production term of  $\widetilde{w''w''}$  is then redistributed to the remaining two Reynolds normal stresses by the pressure redistribution terms, as seen in the previous discussion on budgets of  $\widetilde{u''u''}$  and  $\widetilde{v''v''}$ . The other main contribution to the budget of  $\widetilde{w''w''}$  immediately downstream of the cylindrical cooling film is the convection, which is due to turbulence from the boundary layer and from the front part of the jet being convected toward the rear of the jet itself. These

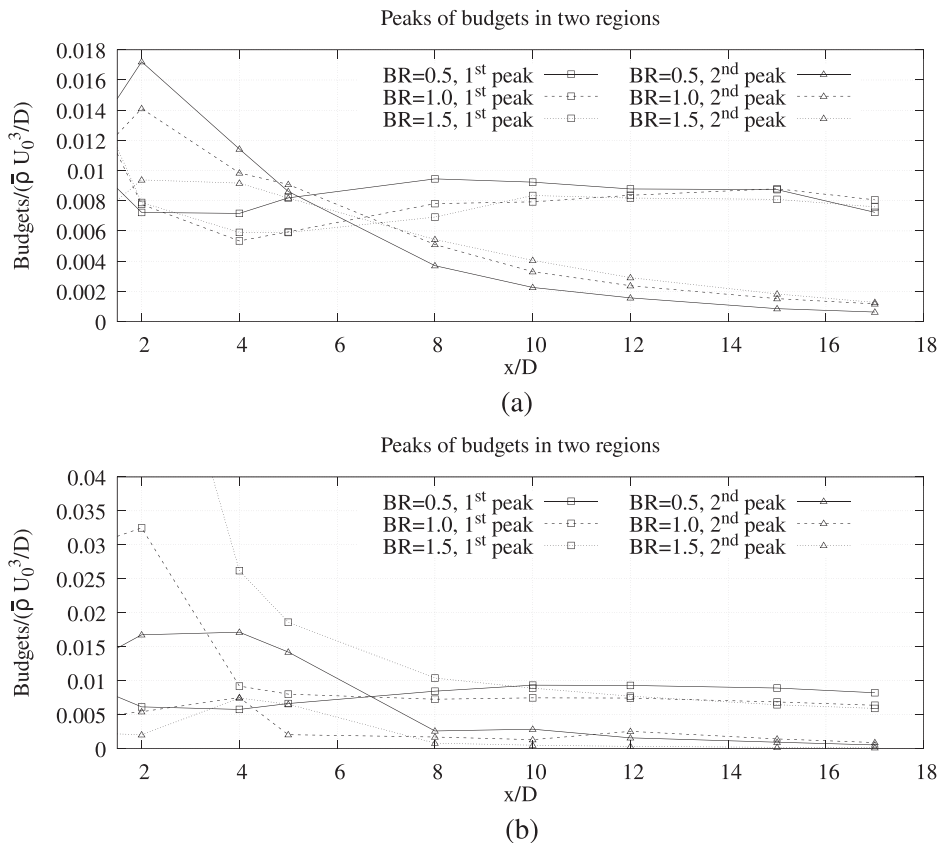


**FIG. 12.** Streamwise development of the peaks in two regions of  $Pr_{uu}$ : (a) fan-shaped hole and (b) cylindrical hole.

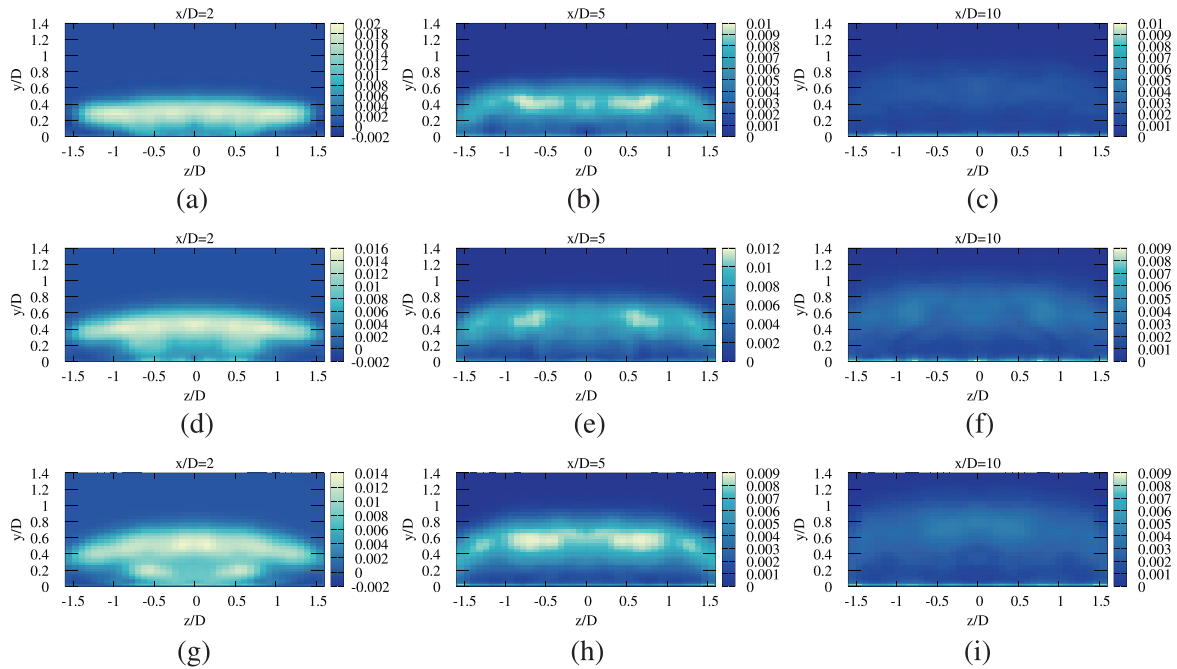


**FIG. 13.** Contours of  $Pr_{uu}$  for fan-shaped films at  $x/D = 2$ ,  $x/D = 5$ , and  $x/D = 10$ : (a)–(c) for  $BR = 0.5$ , (d)–(f) for  $BR = 1.0$ , (g)–(i) for  $BR = 1.5$ ; (a), (d), and (g) at  $x/D = 2$ , (b), (e), and (h) at  $x/D = 5$ , and (c), (f), and (i) at  $x/D = 10$ .

contributions are balanced by pressure redistribution, dissipation, and turbulent diffusion. As the jet evolves downstream to  $x/D = 5$ , the production is reduced but is still the dominant term below the jet. In the upper part of the jet, pressure redistribution acts as a source for the  $w''w''$  budget, where it contributes energy extracted from the mean flow by the  $u''v'' \frac{\partial \bar{u}}{\partial y}$  production term in the  $u''u''$  budget. Below  $y/\delta_{99} \approx 0.3$ , the pressure redistribution acts as a sink for  $w''w''$ , and it sustains the  $u''u''$  and  $v''v''$  fluctuations through energy extracted from the mean flow by the  $w''w'' \frac{\partial \bar{w}}{\partial z}$  term of production. The remaining sinks for  $w''w''$  below  $y/\delta_{99} \approx 0.3$  are the dissipation, turbulent diffusion, and pressure diffusion.

At  $x/D = 10$ , the production peak at  $y/\delta_{99} = 0.2$  is reduced further and has a similar magnitude to the pressure redistribution term further away from the wall. The production of  $w''w''$  is composed of three terms:  $u''w'' \frac{\partial \bar{w}}{\partial x}$ ,  $v''w'' \frac{\partial \bar{w}}{\partial y}$ , and  $w''w'' \frac{\partial \bar{w}}{\partial z}$ . Of these, only  $w''w'' \frac{\partial \bar{w}}{\partial z}$  is non-zero on the  $z = 0$  plane. The remaining two are zero on the centerline because  $u''w''$ ,  $v''w''$ ,  $\frac{\partial \bar{w}}{\partial x}$ , and  $\frac{\partial \bar{w}}{\partial y}$  are all zero. The change in sign of production around  $y/\delta_{99} = 0.3$  is due to  $\frac{\partial \bar{w}}{\partial z}$  changing sign between the part of the flow below and above the cores of the counter-rotating vortex pair. This, in turn, is due to the mean flow pattern depicted in Fig. 6(f).

#### 4. $u''v''$ budget

Figure 10(a) shows the budgets of the Reynolds shear stress  $u''v''$  in the fan-shaped film. Because the Reynolds shear stress  $u''v''$  is negative, the positive terms in this group of figures are the loss, and the negative terms are the gain. At  $x/D = 2$  the budget of  $u''v''$  in the jet layer is dominated by the production, which acts as a source, and by

the redistribution, which acts as a sink. In the proximity of the wall, the dominant terms are pressure diffusion, which acts as a source, and redistribution which acts as a sink. The turbulent diffusion acts by transferring the stress from the wall and from the region above the core of the jet to the region between them.

For the fan-shaped film, at  $x/D = 5$ , the general shapes of the amplitudes are similar. Both the production and pressure diffusion grow with respect to their values at  $x/D = 2$ . They are balanced by the increasing redistribution and the turbulent diffusion below  $y/\delta_{99} = 0.6$ . Above  $y/\delta_{99} = 0.6$ , the structure of the budget remains the same, with the pressure diffusion as the sink balancing the production and turbulent diffusion.

At  $x/D = 10$ , the dominance of the redistribution in the wall-normal direction is extended to  $y/\delta_{99} = 0.7$ . At  $y/\delta_{99} = 0.8$ , the pressure diffusion grows to a peak, which is balanced by turbulent diffusion, redistribution, and production.

In Fig. 10(b), the distribution of the Reynolds stress  $u''v''$  in the cylindrical film case also shows the mark of the area of low turbulence intensities at the core of the jet in the profiles at  $x/D = 2$ . This area appears as a local dip in the magnitude of  $u''v''$  in the  $x/D = 2$  profile around  $y/\delta_{99} = 0.5$ . The Reynolds stress budget at this location is dominated by the production term, which has local maxima at  $y/\delta_{99} \approx 0.3$  and  $y/\delta_{99} \approx 0.8$ . These locations correspond to the lower and upper edges of the jet, respectively. The budget of  $u''v''$  is balanced by pressure redistribution, pressure diffusion, and turbulent diffusion. In the budgets at  $x/D = 5$  and  $x/D = 10$ , the peculiarities of the flow immediately downstream of the film are somewhat reduced, and the budgets display a general structure similar to the one described for the fan-shaped films. The main

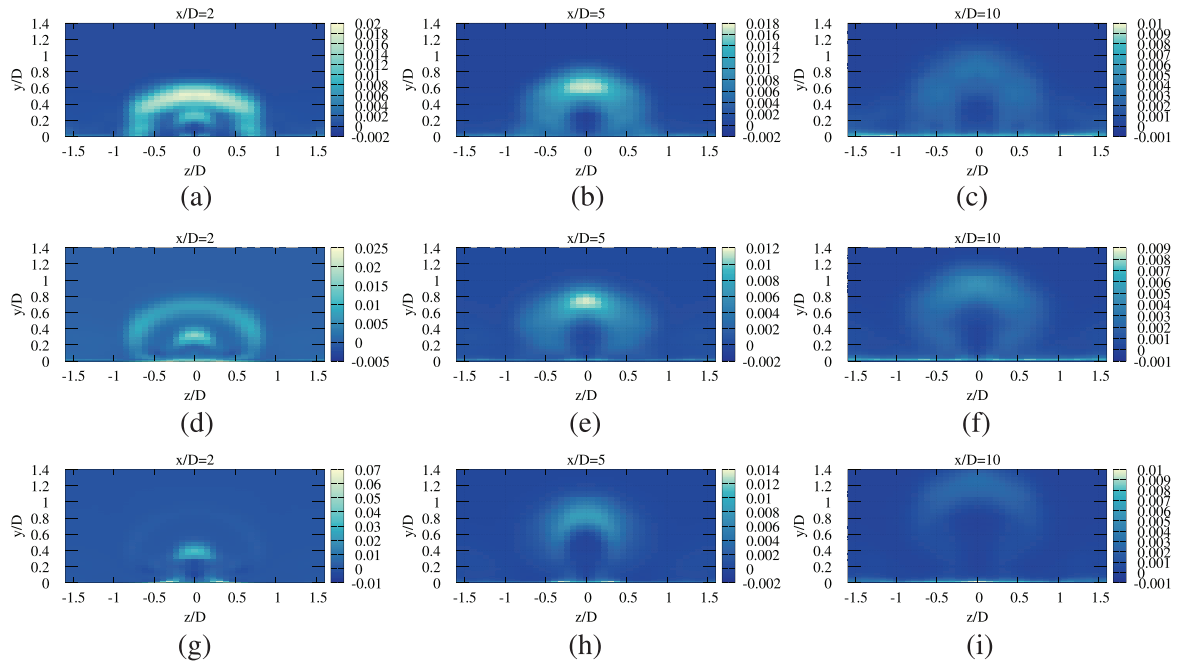


**FIG. 14.** Contours of  $Pr_{uu}$  for cylindrical films at  $x/D = 2$ ,  $x/D = 5$  and  $x/D = 10$ : (a)–(c) for  $BR = 0.5$ , (d)–(f) for  $BR = 1.0$ , (g)–(i) for  $BR = 1.5$ ; (a), (d), and (g) at  $x/D = 2$ , (b), (e), and (h) at  $x/D = 5$ , and (c), (f), and (i) at  $x/D = 10$ .

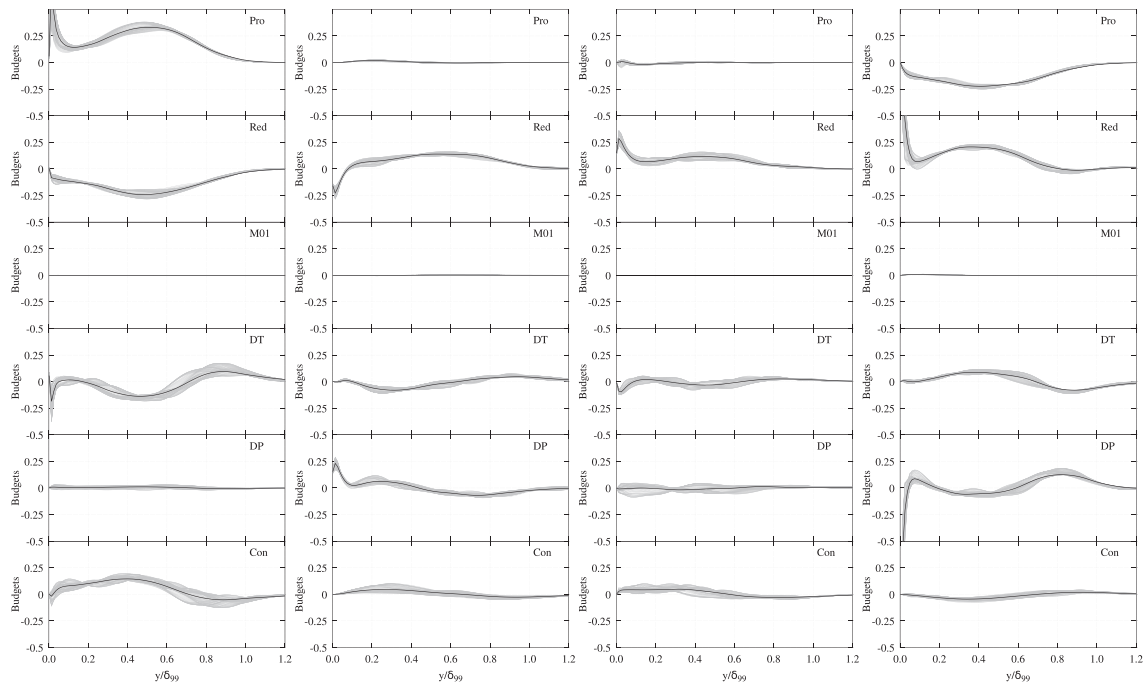


**FIG. 15.** Budget terms scaled by  $(\bar{\rho} \Delta U^3 / ((x/D)^\beta \delta_{99}))$  for fan-shaped film at  $BR = 0.5$ . Gray lines: multiple curves on streamwise positions at  $x/D = 5, \dots, 16$ . Black lines: master curve (average of gray curves). From the left to the right are budgets of  $\overline{u''u''}$ ,  $\overline{v''v''}$ ,  $\overline{w''w''}$ ,  $\overline{u''v''}$ . From the top are production, redistribution, mass flux term, turbulent diffusion, pressure diffusion, and convection.

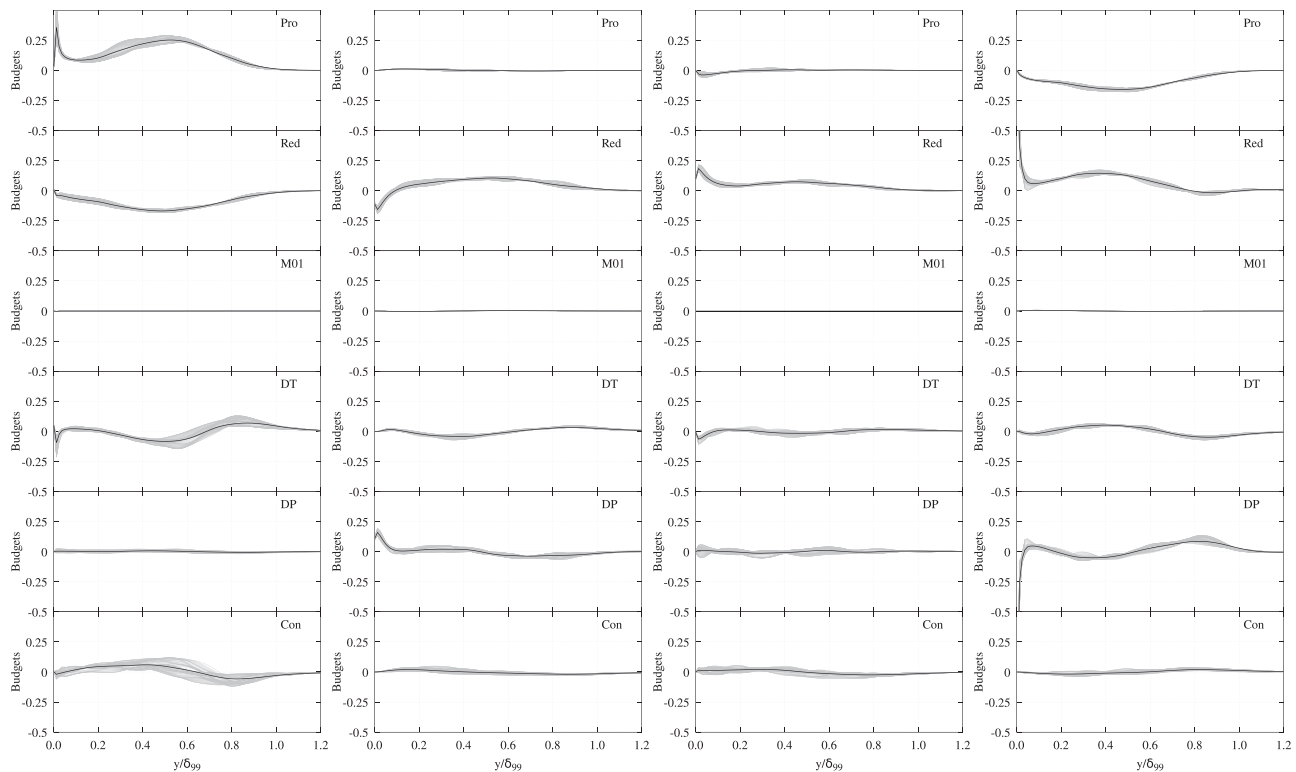


**FIG. 16.** Budget terms scaled by  $(\bar{\rho}\Delta U^3)/((x/D)^\beta \delta_{99})$  for the fan-shaped film at  $BR=1.0$ . Gray lines: multiple curves on streamwise positions at  $x/D = 5, \dots, 16$ . Black lines: master curve (average of gray curves). From the left to the right are budgets of  $u''u''$ ,  $v''v''$ ,  $w''w''$ ,  $u''v''$ . From the top are production, redistribution, mass flux term, turbulent diffusion, pressure diffusion, and convection.

difference between the cylindrical film and the fan-shape film is that the budgets of the Reynolds stress in the former display reduced magnitudes of all terms in the area between the wall layer and  $y/\delta_{99} \approx 0.3$ . This is a consequence of the structure of the flow in the cylindrical film which has a region of lower turbulence intensities between the jet and the wall.

### C. Downstream development

During the discussion on the balancing of different budget terms in Sec. IV B, there are always at least two peaks in the production term of  $u''u''$ . Of these, one is near the wall, and the other is near the upper edge of the wall jet. (In one cylindrical-film case, a third peak appears, but it will not be discussed further in this section.) Figure 12 shows the streamwise evolution of these two peaks in the near-wall region (the first peak) and the jet region (the second peak). The position located by Fig. 12 are on the downstream  $y=0$  slice shown in Fig. 2(c). In the fan-shaped case, the first peak has a nearly constant amplitude downstream of the hole, whereas the second peak decays monotonically. This is because the first peak corresponds to the largest production in a developing boundary layer, and  $u_\tau$  changes very little when the jet flows downstream. The second peak corresponds to the largest production in a free-shear layer and scales approximately with the velocity defect  $\Delta U$  and the distance downstream of the film, as hinted in Sec. IV B.  $\Delta U$  decreases as the jet develops downstream and mixes with

the mainstream. At a position between  $x/D = 5$  and  $x/D = 7$ , the two peaks overlap. At this position, the production of the  $u''u''$  Reynolds normal stress takes place at the same rate in the inner and outer parts of the wall jets.

In the cylindrical case, the first peak has a nearly constant amplitude only in the far field, but in the near field, from  $BR=0.5$  to  $BR=1.5$ , they decay at a rate related to the blowing ratio. The drop in the near field at  $BR=1.0$  and  $1.5$  is caused by the jet lifting off the wall, while at  $BR=0.5$ , the jet is still attached and behaves in a way not dissimilar from the jet of a fan-shaped film. The second peaks in the far field of the cylindrical films have similar changes but with a slower rate of change compared to those in the fan-shaped case. By contrast, the second peaks in the near-field of the cylindrical cooling film have different behaviors: they decay monotonically.

The variation of the peak production on the centerline is shown in Fig. 12, which is in reality part of a more complex three-dimensional pattern.

Distributions of production at several streamwise stations and for several blowing ratios are shown for both fan-shaped and cylindrical films in Figs. 13 and 14. For the fan-shaped film, it can be seen that the production term is distributed along the upper edge of the jet, which appears as a relatively flat region (shown in Fig. 13). Small localized peaks are visible in areas where the jet curves toward the wall at its edges [shown in Figs. 13(a), 13(d), and 13(g)]. For cylindrical films, the production is also distributed around the edge of the film, but this

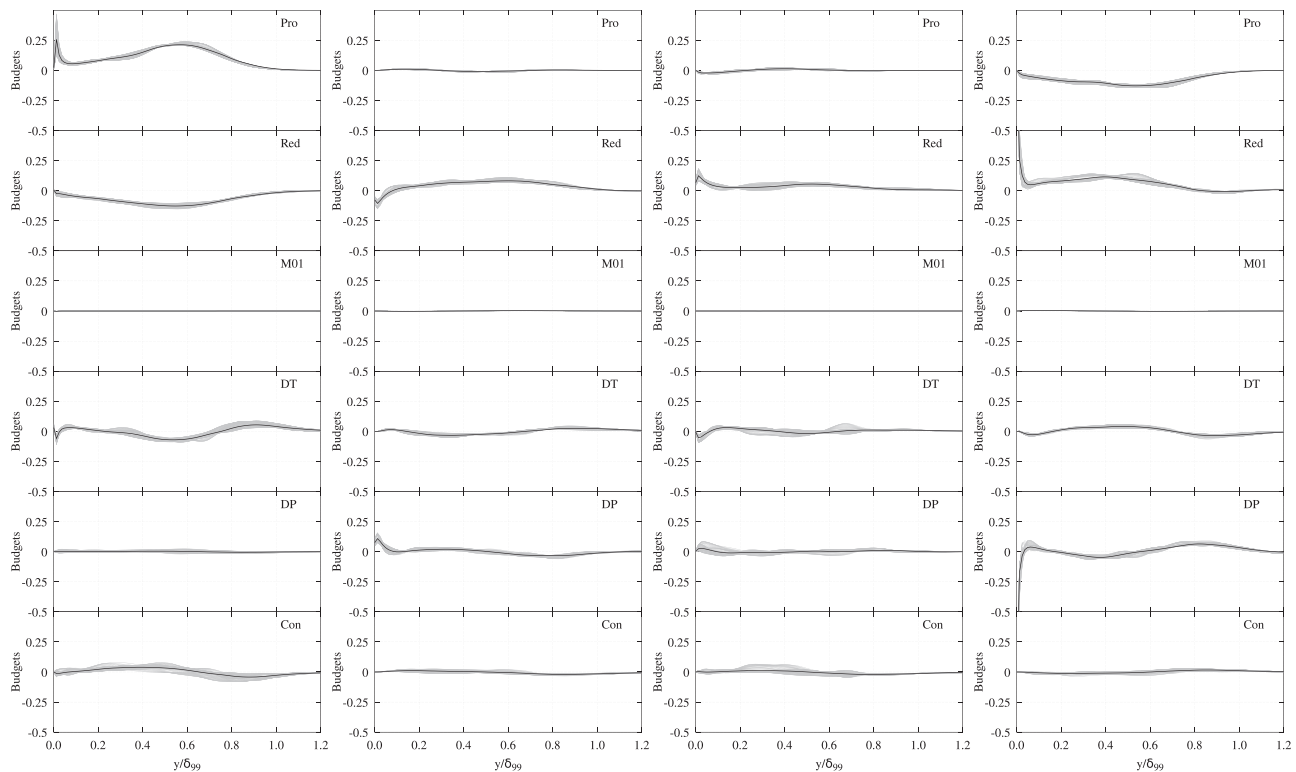


**FIG. 17.** Budget terms scaled by  $(\bar{\rho} \Delta U^3 / ((x/D)^\beta \delta_{99}))$  for the fan-shaped film at  $BR=1.5$ . Gray lines: multiple curves on streamwise positions at  $x/D = 5, \dots, 16$ . Black lines: master curve (average of gray curves). From the left to the right are budgets of  $u''u''$ ,  $v''v''$ ,  $w''w''$ ,  $u''v''$ . From the top are production, redistribution, mass flux term, turbulent diffusion, pressure diffusion, and convection.

is an annular area (shown in Fig. 14). Furthermore, whereas the downstream evolution of the production shows activity only around the edge of the jet, and essentially no production at the core, at  $x/D = 2$ , the attached cylindrical film cases show two distinct areas of activity [shown in Figs. 14(a), 14(d), and 14(g)]. One is located around the outer edge of the jet, and the other is around the boundary between the jet and an area of high turbulence located on the leeward side of the film.

## V. UNIVERSAL SCALING

The self-similarity properties that emerge in the wall-normal profiles of mean quantities and Reynolds stresses are pointed out, as shown by Ref. 16. These self-similarity properties cause graphs of quantities such as mean velocities or turbulence intensities taken at different stream-wise positions to collapse onto each other if appropriately rescaled. The scaling quantities are local quantities and are taken as the thickness of the jet layer and the velocity deficit at a suitably defined location across the layer itself. For films with the attached flow, this location is half of the jet layer thickness; the corresponding velocity scale is the velocity defect evaluated at the half-thickness point, shown in Fig. 11(a). For films with the lifted flow, this location is the position of the largest velocity defect in the upper part of the film, shown in Fig. 11(b). In the latter case, the velocity scale is the largest velocity defect in the upper part of the film.

This scaling, which is based on the integral scales, applies to the outer part of the wall jet, whereas the inner part of the wall jet follows the ordinary wall scaling, albeit with local deviations downstream of the film due to local phenomena like reattachment or adverse pressure gradients.

In this section, it is shown that the external scaling applies not only to the Reynolds stresses but also to their budgets. To this effect, the budget terms taken at locations between  $x/D = 5$  and  $x/D = 16$  are shown in Figs. 15–21. The positions of these lines are indicated by the blue slice as shown in Fig. 2(c). The budget terms are shown at each blowing ratio for the two types of cooling holes. The budget terms are initially rescaled using the scaling factor  $\frac{\Delta U^3}{\delta_{99}} (\frac{x}{D})^{-\beta}$  introduced in Sec. IV B. The wall-normal distance away from the wall is scaled by the transformation

$$y \rightarrow \eta = \frac{\delta_{99} - y}{\delta_{99}}, \quad (18)$$

where  $\delta$  is  $\delta_{99}$  for attached cases. For lifted cases, that is the cylindrical case at  $BR = 1.5$  in this study, the budget terms are also scaled using the scaling factor  $\frac{\Delta U_m^3}{\delta_{99}} (\frac{x}{D})^{-\beta}$ , and the distance away from the wall is correspondingly scaled by the distance of the maximum velocity defect from the wall. All quantities are evaluated on the plane  $z = 0$ .

It can be seen from the results in Figs. 15–21 that the scaling factors above are sufficient to make budget terms collapse into narrow regions. The general trend of the budget terms is easily identified and

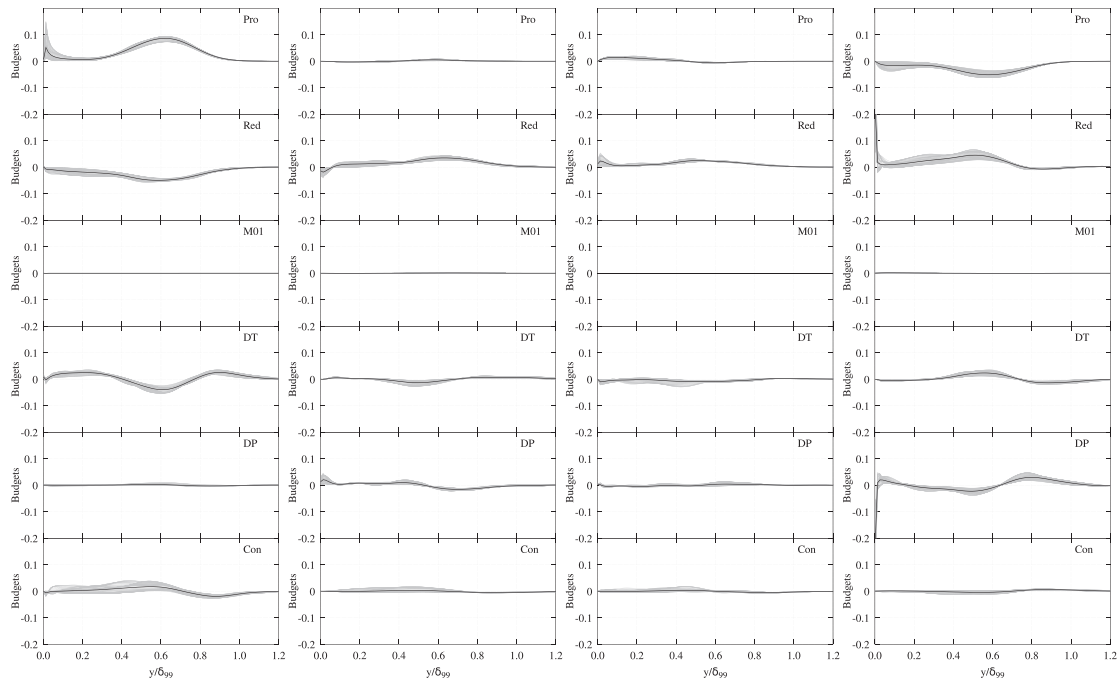


**FIG. 18.** Budget terms scaled by  $(\bar{\rho}\Delta U^3/((x/D)^\beta \delta_{99}))$  for the cylindrical film at  $BR=0.5$ . Gray lines: multiple curves on streamwise positions at  $x/D = 5, \dots, 16$ . Black lines: master curve (average of gray curves). From the left to the right are budgets of  $\overline{u''u''}$ ,  $\overline{v''v''}$ ,  $\overline{w''w''}$ ,  $\overline{u''v''}$ . From the top are production, redistribution, mass flux term, turbulent diffusion, pressure diffusion, and convection.

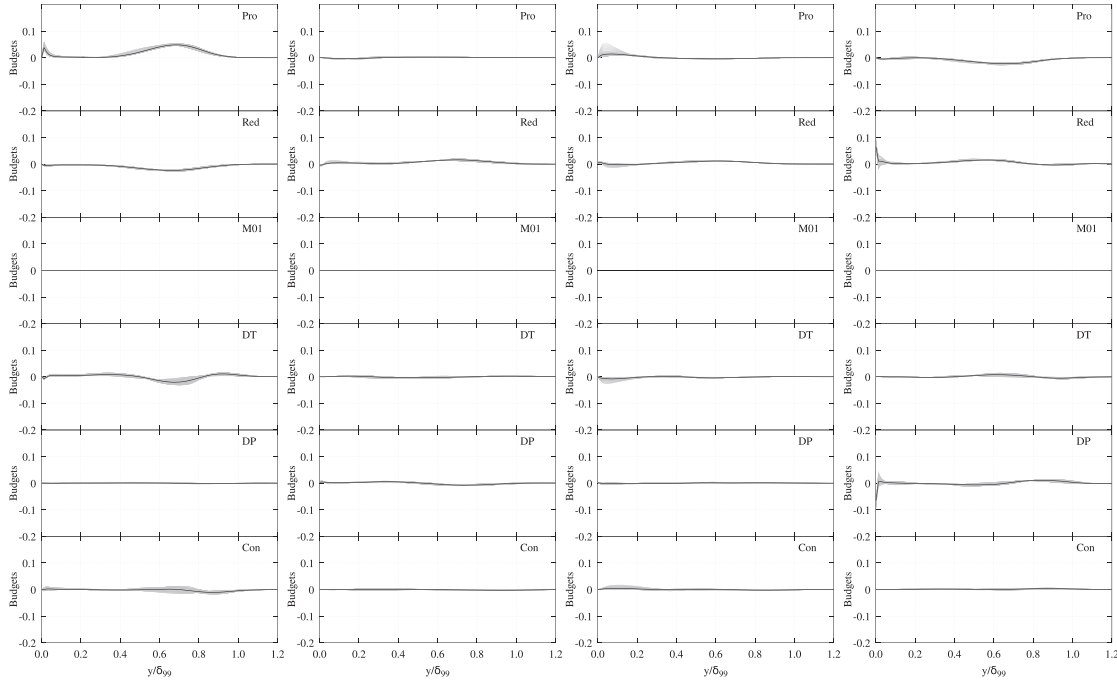


**FIG. 19.** Budget terms scaled by  $(\bar{\rho}\Delta U^3/((x/D)^\beta \delta_{99}))$  for the cylindrical film at  $BR=1.0$ . Gray lines: multiple curves on streamwise positions at  $x/D = 5, \dots, 16$ . Black lines: master curve (average of gray curves). From the left to the right are budgets of  $\overline{u''u''}$ ,  $\overline{v''v''}$ ,  $\overline{w''w''}$ ,  $\overline{u''v''}$ . From the top are production, redistribution, mass flux term, turbulent diffusion, pressure diffusion, and convection.

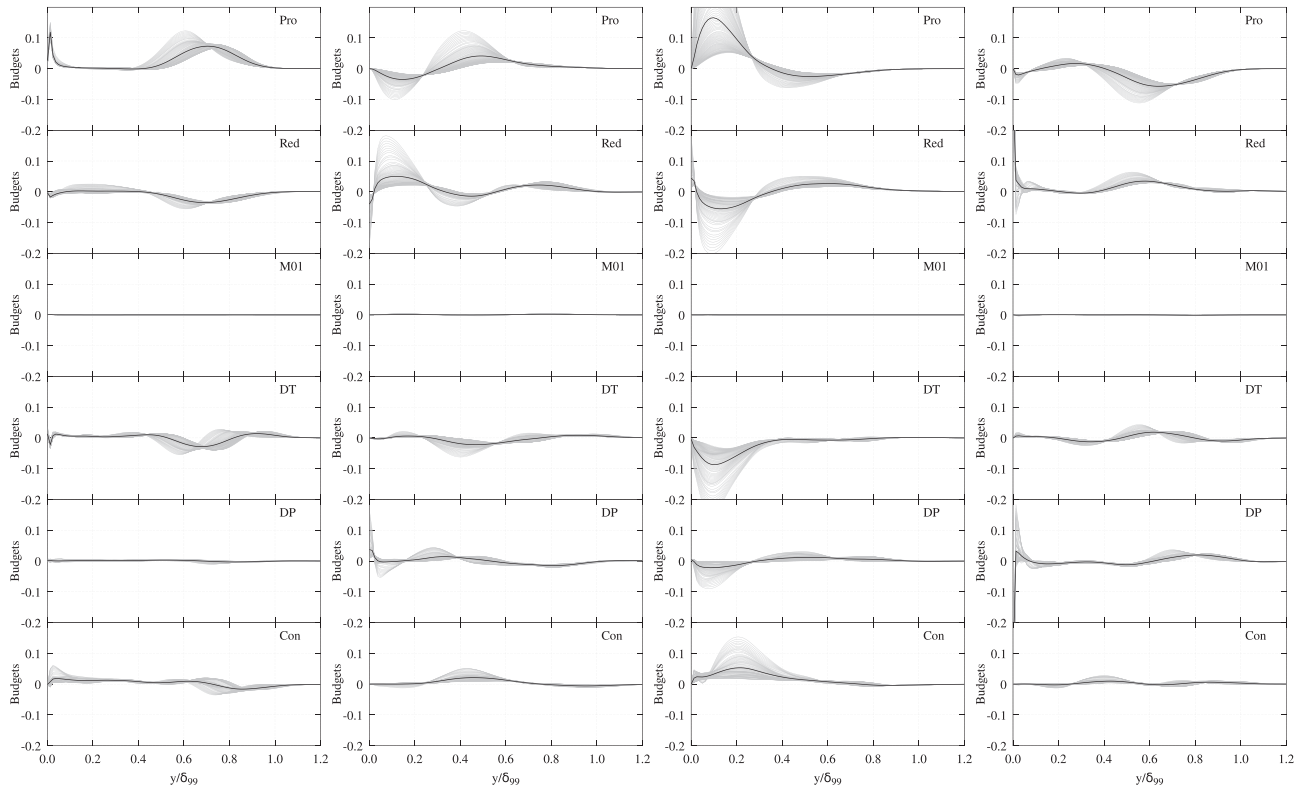


**FIG. 20.** Budget terms scaled by  $(\bar{\rho} \Delta U^3 / ((x/D)^\beta \delta_{99}))$  for the cylindrical film at  $BR = 1.5$ . Gray lines: multiple curves on streamwise positions at  $x/D = 5, \dots, 16$ . Black lines: master curve (average of gray curves). From the left to the right are budgets of  $\overline{u''u''}$ ,  $\overline{v''v''}$ ,  $\overline{w''w''}$ ,  $\overline{u''v''}$ . From the top are production, redistribution, mass flux term, turbulent diffusion, pressure diffusion, and convection.

is shown as master curves in Figs. 15–21. The master curves are obtained by averaging budget terms from all streamwise positions in the wall jet far field at the same nondimensional distance  $\eta$  from the wall. The shape of the master curves is identical to the budgets discussed in Sec. IV B, as these represent the same physical phenomena. The shape and scale of the master curves are also preserved across different blowing ratios if the flow configuration is unchanged. For the lifted case (the cylindrical case at  $BR = 1.5$ ), the scaling using  $\Delta u_m$  and  $\delta_{99}$  and a deduction of  $\delta_m$  performs better collapse of budget profiles. This can be found by comparing Figs. 20 and 21. The magnitude of the scaled budget terms represented by the master curves is also a weak function of the blow ratio, and the entire set of budgets can be represented as a single dataset, dependent only on a nondimensional position and independent of the blowing ratio. Furthermore, the nature of the scaling applies equally well at all blowing ratios and for both geometries. However, the scaling parameter  $\beta$  is sensitive to the flow configuration. For fan-shaped films, the appropriate value of  $\beta$  is 0.5. This results in identical shapes for the velocity (or velocity defect) profiles, the Reynolds stresses, and even the budget terms when rescaled following the proposed scaling. In the case of cylindrical films, the appropriate value of  $\beta$  is 0.9. This value holds equally well for attached cases (lower BR) as for the liftoff case  $BR = 1.5$ . The applicability of an identical scaling exponent  $\beta$  to flows with different arrangements is remarkable. It can be hypothesized that the value of  $\beta$  reflects

the lateral spreading of the jets. In the case of cylindrical films, where the general trend and magnitude of the master curves are preserved across blowing ratios, it is not possible to identify a unique shape for each term that can be applied independently of the blowing ratio. This observation reflects the fact that when the same fundamental processes are taking place, the scaling exponent maintains the same value.

## VI. CONCLUSION

A detailed study of the structure of normal and shear Reynolds stress budgets has been presented for fan-shaped and cylindrical cooling films. It is shown that the structure of the wall jets produced by film-cooling devices can be divided into a near field and a far field. The near field is dominated by the changes in the structure of the jet as it merges with the main flow. The far field is dominated by the gradual mixing of the jet with the surrounding fluid. The far-field approaches self-similar behavior in the mean flow profiles and an approximately self-similar behavior can be achieved in the budget terms as long as an additional scaling factor containing the distance from the position of a maximum velocity defect is introduced. The power law in this additional scaling factor is dependent on the film geometry only and applies over a wide variety of blowing ratios and flow regimes.

The results show that in fan-shaped films, the general structure of the Reynolds stress budgets is not very different between the near and the far field. The opposite is true for cylindrical films, where the near

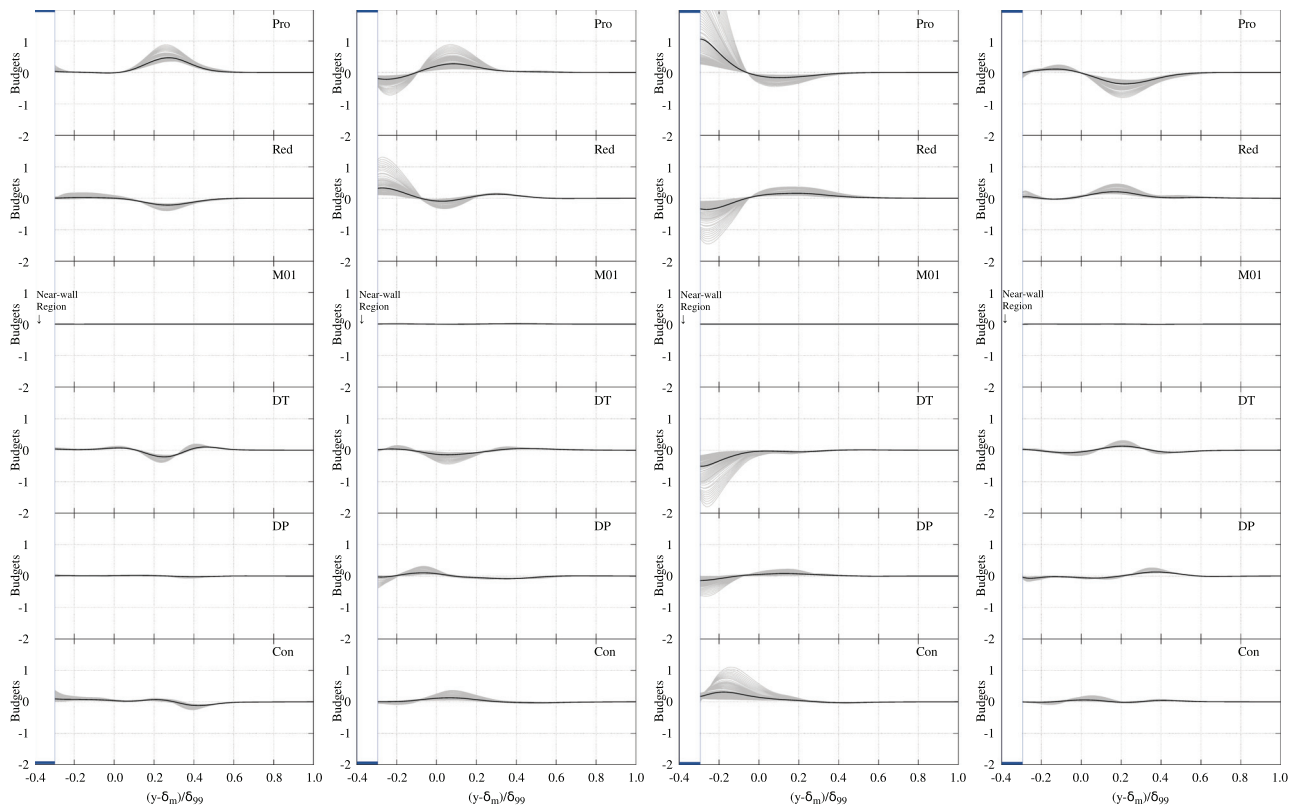


**FIG. 21.** Budget terms scaled by  $(\bar{\rho}\Delta U_m^3)/((x/D)^\beta\delta_{99})$  for the cylindrical film at  $BR=1.5$ . Gray lines: multiple curves on streamwise positions at  $x/D = 5, \dots, 16$ . Black lines: master curve (average of gray curves). From the left to the right are budgets of  $\overline{u'u'}$ ,  $\overline{v'v'}$ ,  $\overline{w'w'}$ ,  $\overline{u'v'}$ . From the top are production, redistribution, mass flux term, turbulent diffusion, pressure diffusion, and convection.

field is dominated by localized regions of high turbulence intensity and turbulent shear stress. These regions are found immediately downstream of the film and are characterized by high levels of anisotropy, due to the presence of the wall and of the confinement caused by the jet. Also, the main source of turbulent kinetic energy in the outer part of the jets issuing from both films is the production term in the  $\overline{u'u'}$  budget. Energy extracted from the mean flow through this term is then fed into the normal Reynolds stresses via pressure redistribution terms. In the regions of high anisotropy immediately downstream of cylindrical films, most of the turbulent kinetic energy production takes place through the work done by the normal Reynolds stress  $\overline{w'w'}$  against the spanwise derivative of the mean spanwise velocity  $w$ . Energy extracted by this work is then fed to the  $\overline{u'u'}$  and  $\overline{v'v'}$  normal stresses via pressure redistribution. In cylindrical films, the production of turbulent kinetic energy via the term  $\overline{w'w'} \frac{\partial w}{\partial z}$  is still active far downstream, and its sign is determined by the sign of the derivative  $\frac{\partial w}{\partial z}$ . The sign of this derivative, in turn, is determined by the position of the cores of the pair of counter-rotating vortices locating the jet. This process is absent in the jet produced by the fan-shaped film, where  $\frac{\partial w}{\partial z}$  is small because the system of counter-rotating vortices is less well-defined and sits much farther apart from the centerline and much closer to the wall.

It has been known for a long time that far downstream of their origin, two-dimensional wall jets obey partial similarity laws, which

apply to different parts of the flow field. The discovery of modified scaling laws for the outer part of the Reynolds stress budget indicates that such modified scaling laws should exist in the far field for three-dimensional wall jets as well. The existence of such scaling laws, in turn, is a clear indication that modeling difficulties usually encountered in modeling film-cooling devices originated in the near field where history effects and anisotropy are more pronounced. This observation also explains why the flows issuing from cylindrical films are more difficult to predict and more sensitive to modeling assumptions than those from fan-shaped films and similar devices. A modified scaling law for the budgets has not previously been reported in the literature for film-cooling flows. Such a theory will be published in a future study.<sup>26</sup>

In terms of the implication for future study, the results clearly demonstrate anisotropy of stress and budget terms. This needs to be handled in future modeling attempts. The results also indicate self-similarity properties that can be invoked when setting constants. It is likely that the near field shows high sensitivity to film geometry, and a detailed analysis of the stress field will be required for alternative film styles. This is a limitation of this study. However, the far-field behavior can be shown to follow scaling laws as consequences of the conservation of mass momentum and energy and is likely to be a universal conclusion.

## ACKNOWLEDGMENTS

Rolls-Royce plc is gratefully acknowledged for supporting this work and for granting permission for its publication. The paper was finished under Grant No. DFR03150. The authors sincerely thank Romero Eduardo, Frederic Goenaga, and Cristian Orozco Pineiro in Rolls-Royce plc for helpful discussion. The authors also acknowledge the use of the University of Oxford Advanced Research Computing (ARC) facility in carrying out this work. <http://dx.doi.org/10.5281/zenodo.22558>. Part of this work was also performed using resources provided by the Cambridge Service for Data Driven Discovery (CSD4) operated by the University of Cambridge Research Computing Service ([www.csd3.cam.ac.uk](http://www.csd3.cam.ac.uk)), provided by Dell EMC and Intel using Tier-2 funding from the Engineering and Physical Sciences Research Council (Capital Grant No. EP/T022159/1), and DiRAC funding from the Science and Technology Facilities Council ([www.dirac.ac.uk](http://www.dirac.ac.uk)).

## AUTHOR DECLARATIONS

## Conflict of Interest

The authors have no conflicts to disclose.

## Author Contributions

**Muting Hao:** Conceptualization (equal); Data curation (equal); Formal analysis (equal); Investigation (equal); Methodology (equal); Software (equal); Validation (equal); Visualization (equal); Writing – original draft (equal); Writing – review & editing (equal). **Luca di Mare:** Conceptualization (equal); Funding acquisition (equal); Investigation (equal); Project administration (equal); Supervision (equal); Writing – review & editing (equal).

## DATA AVAILABILITY

The data that support the findings of this study are available from the corresponding author upon reasonable request.

## REFERENCES

- <sup>1</sup>A. Hoda and S. Acharya, “Predictions of a film coolant jet in crossflow with different turbulence models,” *J. Turbomach.* **122**, 558–569 (1999).
- <sup>2</sup>S. V. Patankar, D. K. Basu, and S. A. Alpay, “Prediction of the three-dimensional velocity field of a deflected turbulent jet,” *J. Fluids Eng.* **99**, 758–762 (1977).
- <sup>3</sup>S. E. Guarini, R. D. Moser, K. Shariff, and A. Wray, “Direct numerical simulation of a supersonic turbulent boundary layer at Mach 2.5,” *J. Fluid Mech.* **414**, 1–33 (2000).
- <sup>4</sup>P. G. Huang, G. N. Coleman, and P. Bradshaw, “Compressible turbulent channel flows: DNS results and modelling,” *J. Fluid Mech.* **305**, 185–218 (1995).
- <sup>5</sup>S. Ghosh, H. Foysi, and R. Friedrich, “Compressible turbulent channel and pipe flow: Similarities and differences,” *J. Fluid Mech.* **648**, 155–181 (2010).
- <sup>6</sup>M. A. Vyas, D. A. Yoder, and D. V. Gaitonde, “Reynolds-stress budgets in an impinging shock-wave/boundary-layer interaction,” *AIAA J.* **57**, 4698–4714 (2019).
- <sup>7</sup>G. Nicholson, J. Huang, L. Duan, M. M. Choudhari, and R. D. Bowersox, “Simulation and modeling of hypersonic turbulent boundary layers subject to favorable pressure gradients due to streamline curvature,” AIAA Paper No. 2021-1672 (2021).
- <sup>8</sup>S. Hoyas and J. Jiménez, “Reynolds number effects on the Reynolds-stress budgets in turbulent channels,” *Phys. Fluids* **20**, 101511 (2008).
- <sup>9</sup>F. Muldoon and S. Acharya, “Analysis of k and epsilon budgets for film cooling using direct numerical simulation,” *AIAA J.* **44**, 3010–3021 (2006).
- <sup>10</sup>R. Zhi, Z. Li, F. Wen, L. Su, and S. Wang, “Research on performance predictions using single-hole film cooling based on PointNet,” *Phys. Fluids* **35**, 025108 (2023).
- <sup>11</sup>W. Zhou, H. Chen, Y. Liu, X. Wen, and D. Peng, “Unsteady analysis of adiabatic film cooling effectiveness for discrete hole with oscillating mainstream flow,” *Phys. Fluids* **30**, 127103 (2018).
- <sup>12</sup>Z. Zhang, X. Wu, and X. Wang, “Near-wall vortices and thermal simulation of coupled-domain transpiration cooling by a recursive regularized lattice boltzmann method,” *Phys. Fluids* **34**, 107105 (2022).
- <sup>13</sup>R. Qiao, K. Mu, X. Luo, and T. Si, “Instability and energy budget analysis of viscous coaxial jets under a radial thermal field,” *Phys. Fluids* **32**, 122103 (2020).
- <sup>14</sup>I. Rogachevskii, N. Kleorin, and S. Zilitinkevich, “Energy- and flux-budget theory for surface layers in atmospheric convective turbulence,” *Phys. Fluids* **34**, 116602 (2022).
- <sup>15</sup>N. Kleorin, I. Rogachevskii, and S. Zilitinkevich, “Energy and flux budget closure theory for passive scalar in stably stratified turbulence,” *Phys. Fluids* **33**, 076601 (2021).
- <sup>16</sup>M. Hao and L. di Mare, “Reynolds stresses and turbulent heat fluxes in fan-shaped and cylindrical film cooling holes,” *Int. J. Heat Mass Transfer* **214**, 124324 (2023).
- <sup>17</sup>M. Gritsch, A. Schulz, and S. Wittig, “Adiabatic wall effectiveness measurements of film-cooling holes with expanded exits,” *J. Turbomach.* **120**, 549–556 (1998).
- <sup>18</sup>M. Gritsch, A. Schulz, and S. Wittig, “Discharge coefficient measurements of film-cooling holes with expanded exits,” *J. Turbomach.* **120**, 557–563 (1998).
- <sup>19</sup>M. Hao, “Numerical methods for unsteady film cooling in gas turbine,” Ph.D. thesis (The University of Oxford, 2023).
- <sup>20</sup>M. Hao, F. Wang, J. Hope-Collins, M. E. Rife, and L. di Mare, “Template-based hexahedral mesh generation for turbine cooling geometries,” in *ASME Turbo Expo: Turbomachinery Technical Conference and Exposition* (American Society of Mechanical Engineers, 2020).
- <sup>21</sup>M. Čada and M. Torrilhon, “Compact third-order limiter functions for finite volume methods,” *J. Comput. Phys.* **228**, 4118–4145 (2009).
- <sup>22</sup>M. Hao, J. Hope-collins, and L. di Mare, “Generation of turbulent inflow data from realistic approximations of the covariance tensor,” *Phys. Fluids* **34**, 115140 (2022).
- <sup>23</sup>K. W. Thompson, “Time dependent boundary conditions for hyperbolic systems,” *J. Comput. Phys.* **68**, 1–24 (1987).
- <sup>24</sup>T. B. Gatski and J.-P. Bonnet, “Measurement and analysis strategies,” in *Compressibility, Turbulence and High Speed Flow* (Elsevier, 2009), pp. 79–116.
- <sup>25</sup>P. R. Spalart, “Direct simulation of a turbulent boundary layer up to  $Re_\theta = 1410$ ,” *J. Fluid Mech.* **187**, 61–98 (1988).
- <sup>26</sup>M. Hao and L. di Mare, “Scaling and similarity laws in three-dimensional wall jets,” *Phys. Fluids* **35**, 075102 (2023).